Polyion Complex Micelles of pDNA with Acetal-poly(ethylene glycol)-poly(2-(dimethylamino)ethyl methacrylate) Block Copolymer as the Gene Carrier System: Physicochemical Properties of Micelles Relevant to Gene Transfection Efficacy

Daisuke Wakebayashi,[†] Nobuhiro Nishiyama,[†,‡] Keiji Itaka,[†,§] Kanjiro Miyata,[†] Yuichi Yamasaki,[†] Atsushi Harada,[†] Hiroyuki Koyama,[‡] Yukio Nagasaki,[∥] and Kazunori Kataoka*[,†]

Department of Materials Science and Engineering, Graduate School of Engineering, The University of Tokyo, 7-3-1 Hongo, Bunkyo-ku, Tokyo 113-8656, Japan, Department of Clinical Vascular Regeneration, Graduate School of Medicine, The University of Tokyo, 7-3-1 Hongo, Bunkyo-ku, Tokyo 113-8655, Japan, Department of Orthopedic Surgery, Faculty of Medicine, The University of Tokyo, 7-3-1 Hongo, Bunkyo-ku, Tokyo 113−8655, Japan, and Department of Materials Science, Tokyo University of Science, 2641 Yamazaki, Noda, Chiba, 278-8510, Japan

Received March 1, 2004; Revised Manuscript Received June 24, 2004

An acetal-poly(ethylene glycol)-poly(2-(dimethylamino)ethyl methacrylate) (acetal-PEG-PAMA) block copolymer spontaneously associated with plasmid DNA (pDNA) to form water-soluble complexes (polyion complex micelle: PIC micelle) in aqueous solution. Physicochemical characteristics and transfection efficiency of the PIC micelles thus prepared were studied here, focusing on the residual molar mixing ratio (N/P ratio) of AMA units in acetal-PEG-PAMA to the phosphate units in pDNA. With the N/P ratio increasing to unity, acetal-PEG-PAMA cooperatively formed complex micelles with pDNA through electrostatic interaction, allowing pDNA to condense effectively. Dynamic light scattering measurements revealed that the PIC micelle at N/P ≥ 3 had a constant size of approximately 90−100 nm. Eventually, acetal-PEG-PAMA/pDNA micelles underwent no precipitation even after long-term storage for more than 1 month at all N/P ratios. The PIC micelles were stable even in the presence of excess polyanions, poly(vinyl sulfate), in contrast to polyplexes based on the PAMA homopolymer, yet this stabilization effect was highly dependent on the N/P ratio to reach a plateau at N/P = 3−4. This character may be attributed to the increased hydrophobicity in the vicinity of the complexed pDNA. Furthermore, the pDNA in the micelle was adequately protected from DNase I attack. The transfection ability of the PIC micelles toward 293 cells was remarkably enhanced with an increasing N/P ratio as high as 25. The ζ-potential of the micelles with a high N/P ratio was an appreciably large positive value, suggesting a noncooperative micelle formation. This deviated micellar composition with an excess cationic nature as well as the presence of free acetal-PEG-PAMA may play a substantial role in the enhanced transfection efficiency of the PIC micelle system in the high N/P ratio (~25) region.

1. Introduction

Gene therapy has been receiving much attention as a promising treatment for genetic and intractable diseases.[1−4] Particularly, it is strongly desired to achieve in vivo gene therapy in which a therapeutic gene is introduced into target cells through topical or systemic administration. One of the major requirements for in vivo gene therapy is the development of a gene vector system which can safely and effectively deliver a therapeutic gene into specific cells and can then achieve regulated gene expression. Although recombinant viruses, which have been mainly used in clinical treatment, provide a high level of gene transfer due to their inherent ability for infection, they have many disadvantages in terms of safety such as the induction of immunogenic responses, the risk of virus-mediated random integration, and recombination with wild-type viruses. Furthermore, their universal utility is limited due to a restriction in the size of compartmentalized DNA, the difficulty of scale-up, and the high cost of manufacturing. These essential disadvantages of a virus vector motivate the development of safe and effective nonviral vector systems.

Ion-complexed nonviral vectors such as lipoplex and polyplex, in which cationic lipids or polymers, respectively, associate with DNA through electrostatic interaction, are the most widely studied for both in vitro and in vivo transfection.[5−8] Nevertheless, lipoplex and polyplex have a problem in that they readily form water-insoluble aggregates under a charge stoichiometric condition. Water-soluble ion

* To whom correspondence should be addressed. E-mail: kataoka@bmw.t.u-tokyo.ac.jp. Phone: +81-3-5841-7138. Fax: +81-3-5841-7139.
† Graduate School of Engineering, The University of Tokyo.
‡ Graduate School of Medicine, The University of Tokyo.
§ Faculty of Medicine, The University of Tokyo.
∥ Tokyo University of Science.

10.1021/bm040009j CCC: $27.50
Published on Web 09/25/2004

complexes may be prepared by mixing an excess cationic component with DNA,[9,10] and the cationic nature of the complexes facilitates cellular uptake of condensed DNA via electrostatic adsorption onto anionic cell surfaces. On the other hand, systemic injection of cationic complexes is likely to cause nonspecific disposition, resulting in their rapid clearance from the bloodstream. Therefore, it is difficult to achieve effective gene targeting by cationic vector systems through systemic administration. Furthermore, enhanced toxicity was often encountered with these cationic vectors.

These contradictory issues between solubility and biocompatibility may be overcome by surrounding the polyplexes with nonionic and hydrophilic polymers such as poly(ethylene glycol) (PEG).[11-14] A PEGylated polyplex shows improved water solubility even under a charge stoichiometric condition, allowing reduction of nonspecific disposition as well as toxicity. Indeed, water-soluble complexes of a poly(ethylene glycol)-poly(L-lysine) (PEG-PLL) block copolymer with DNA (polyion complex micelle: PIC micelle) achieved highly improved stability in a serum-containing medium compared to PLL/pDNA complexes or a lipoplex and even showed prolonged blood circulation in experimental animals.[15-18] Eventually, PEG-PLL/pDNA micelles achieved appreciable gene expression in the liver.[18] Improved blood circulation as well as enhanced in vivo gene expression was further confirmed for several PEGylated polyplexes.[19,20]

Disposition in the body of PEGylated polyplexes, including PIC micelles, is determined mainly by the surface properties, yet the transfection efficiency is highly dependent on the chemical structure of the core forming polycations.[8,21] Polycations with varying chemical structure such as DEAE-dextran, PLL, polyethylenimine (PEI), poly(2-(dimethylamino)ethyl methacrylate) (PAMA), and chitosan have so far been investigated as cationic components of polyplexes.[22-27] Differences in chemical properties, including charge density, flexibility, hydrophobicity, and the structure of the cationic group, substantially affect the physicochemical nature of the polyplexes and eventually determine the transfection ability.[6,28] PAMA is one of the promising polycations expected to achieve a buffering effect due to its relatively low pK_a (pK_a = 7.4−7.8).[21,29] Effective transfection was indeed achieved using PAMA/DNA polyplexes in the absence of a lysosomotropic agent such as chloroquine.[25,26] Furthermore, PAMA has lower cytotoxicity than PLL.[26] These interesting properties of PAMA make it worth choosing as the cationic segment of the block copolymer to form PIC micelle vectors, leading to the development of the novel synthesis method for a PEG-PAMA block copolymer as reported previously.[30] In this previous study, the acetal group, which can be readily transformed into a reactive aldehyde group by a gentle acid treatment in aqueous medium, was introduced into the PEG terminal of the PEG-PAMA block copolymer to allow the conjugation of cell-specific ligands, such as sugars and peptides, on the surface of the micelles, which may have potential utilities as a targetable vector in gene delivery.[31]

Here, we report the physicochemical characteristics of PIC micelles from acetal-PEG-PAMA and plasmid DNA (pDNA) with various mixing ratios. Focus is placed on the relationship between these characteristics and the transfection efficiency toward cultured cells (293 cells) to clarify the structural features of the acetal-PEG-PAMA/pDNA micelles important for their use as a gene vector system.

2. Experimental Section

2.1. Materials. The acetal-PEG-PAMA block copolymer was prepared as described previously.[30] In this study, the molecular weight of the PEG segment and the polymerization degree of the PAMA segment of the block copolymer were fixed at 5100 g/mol and 63, respectively. PAMA homopolymer was obtained by the anionic polymerization of AMA using potassium ethoxide as an initiator.[32] The polymerization degree of PAMA was determined to be 64 (M_n = 10 000 g/mol, M_w/M_n = 1.35) by size exclusion chromatography (SEC). Standard polystyrenes were used for the calibration.

pGL3-Luc plasmid DNA was purchased from Promega (Madison, WI). Plasmid DNA (pDNA) was amplified in competent DH5α *Escherichia coli* and purified by a HiSpeed Plasmid Maxi Kit (QIAGEN, Germany). The concentration of prepared pDNA was determined by measuring the absorbance at 260 nm using a UV/vis spectrophotometer (Jasco, V-550, Tokyo, Japan). The purity of the pDNA was confirmed by 0.9% agarose gel electrophoresis as well as by measuring the absorbance ratio of pDNA solution at 260/280 nm. Potassium poly(vinyl sulfate) (degree of polymerization (DP) > 1500) (PVSK) was purchased from Wako Pure Chemical (Osaka, Japan). LipofectAMINE reagent was purchased from GIBCO-BRL (Burlington). Hydroxychloroquine was purchased from Acros Organics (NJ). Fetal bovine serum (FBS) with heat-inactivating treatment was purchased from ICN Biomedicals, Inc. (OH). The luciferase assay kit was a product of Promega. The Micro BCA protein assay reagent kit was purchased from Pierce (Rockford, IL). For other reagents, commercial special grade reagents were used as received.

2.2. Preparation of Polyion Complex Micelles and PAMA/pDNA Polyplexes. Acetal-PEG-PAMA and pGL3-Luc plasmid DNA (pDNA) were dissolved separately in 10 mM Tris-HCl buffer (pH 7.4). Acetal-PEG-PAMA solution in varying concentrations was then added to the pDNA solution at a fixed concentration (50 μg/mL) to form polyion complex (PIC) micelles of different compositions. To the mixed solution was added 10 mM Tris-HCl buffer (pH 7.4) to adjust the final DNA concentration to 30 μg/mL. The resulting solution was kept at ambient temperature overnight. The residual molar mixing ratio (N/P ratio) was defined as the ratio of the residual molar concentration of AMA units in acetal-PEG-PAMA to that of the phosphate groups in pDNA (=[AMA units in acetal-PEG-PAMA]/[phosphate groups in pDNA]). PAMA/pDNA polyplexes were also prepared in a way similar to that for the PIC micelles except for being subjected to a biological assay 30−60 min after the mixing of PAMA and pDNA.

2.3. Gel Retardation Assay. PIC micelle solutions prepared at various N/P ratios (30 μg of pDNA/mL) were diluted to 10 μg of pDNA/mL by 10 mM Tris-HCl buffer

and then electrophoresed at 2.8 V/cm with 0.6 w/w % agarose gel in buffer (3.3 mM Tris-acetic acid (pH 7.4), 1.7 mM sodium acetate, 1 mM EDTA2Na). The migrated pDNA was visualized by soaking the gel in distilled water containing ethidium bromide (0.5 μg/mL).

2.4. Ethidium Bromide Exclusion Assay. The effect of the N/P ratio on the degree of pDNA condensation in PIC micelles was estimated from the reduction in fluorescence intensity of ethidium bromide (EtBr) due to the exclusion from DNA. PIC micelle solutions (30 μg of pDNA/mL) prepared at various N/P ratios were adjusted to 20 μg of pDNA/mL with 0.4 μg of EtBr/mL by adding 10 mM Tris-HCl buffer containing EtBr. The ratio of the residual molar concentration of EtBr to that of the base pair in pDNA was 0.033. The solutions were incubated at ambient temperature overnight. Fluorescence measurements of sample solutions were carried out at 25.0 ± 0.2 °C using a spectrofluorometer (Jasco, FP-777). Excitation (Ex) and emission (Em) wavelengths were 510 and 590 nm, respectively. Results were expressed as relative fluorescence intensity. The fluorescence of pDNA solution with EtBr was set at 100%, measured against a background of EtBr without pDNA.

2.5. Dynamic Light Scattering Measurements. The size of PIC micelles was evaluated by dynamic light scattering (DLS). Sample solutions with various N/P ratios in 10 mM Tris-HCl buffer (pH 7.4) were adjusted to a concentration of 30 μg of pDNA/mL. DLS measurements were carried out at 25.0 ± 0.2 °C using a DLS-7000 instrument (Otsuka Electronics, Hirakata, Japan) with a vertically polarized incident beam of 488 nm wavelength from an Ar ion laser. A scattering angle of 90° was used in these measurements. Data were analyzed by a cumulant method as reported in detail previously.[33]

2.6. ζ-Potential Measurements. The ζ-potential of PIC micelles was evaluated by the laser-doppler electrophoresis method. Sample solutions were prepared similarly to DLS measurements. The ζ-potential measurements were carried out at 25.0 ± 0.2 °C using an ELS-6000 instrument (Otsuka Electronics) equipped with a He−Ne ion laser (633 nm). A scattering angle of 20° was used in these measurements. From the obtained electrophoretic mobility, the ζ-potential was calculated using the Smoluchowski equation as follows:

$$\zeta = 4\pi\eta u/\epsilon$$

Here u is the electrophoretic mobility, η is the viscosity of the solvent, and ϵ is the dielectric constant of the solvent. The results reported are expressed as mean values (±SD) of three experiments.

2.7. Nuclease Resistance of pDNA Complexed with Acetal-PEG-PAMA. Either of pDNA or acetal-PEG-PAMA/pDNA micelle (20 μg/mL) prepared at N/P = 1.25 in 10 mM Tris-HCl buffer, pH 7.4, containing 5 mM $MgSO_4$ was incubated with DNase I (0.05 U) at 37 °C. After a defined time of incubation, 20 μL of the solution was treated with 5 μL of 200 mM ethylenediaminetetraacetic acid (EDTA) solution to inactivate DNase I. An excess of potassium poly(vinyl sulfate) (PVSK) solution in 100 mM AcONa−AcOH buffer (pH 5) was then added to the micelle solution to dissociate the PIC micelle. After overnight incubation of the mixtures, each sample was electrophoresed through 0.9% agarose gel in 60 mM AcONa−AcOH buffer containing 1 mM EDTA (pH 5). The migrated pDNA was visualized by soaking the gel into EtBr solution (0.5 μg/mL) and analyzed using Luminous Imager (Aisin cosmos, Aichi, Japan).

2.8. Stability of Acetal-PEG-PAMA/pDNA Micelles and PAMA/pDNA Polyplexes on the Exchange Reaction with Polyanion. The release of pDNA from PIC micelles and polyplexes at pH 7.4 was evaluated through the exchange reaction with potassium poly(vinyl sulfate) (PVSK) as the polyanion. PVSK was dissolved in 10 mM Tris-HCl buffer (pH 7.4). Buffer solution with or without a large excess of PVSK was added to the same volume of acetal-PEG-PAMA/pDNA micelles or PAMA/pDNA polyplexes solution (30 μg of pDNA/mL) prepared at various mixing ratios (N/P = 1.25, 2.5, 3.75, 5) in 10 mM Tris-HCl buffer (pH 7.4). After overnight incubation at room temperature, an assay at pH 7.4 was done by electrophoresing each sample with or without PVSK through a 0.6% agarose gel in buffer (3.3 mM Tris-acetic acid (pH 7.4) + 1.7 mM sodium acetate + 1 mM EDTA2Na). pDNA in the gel was visualized by soaking the gel in distilled water containing EtBr (0.5 μg/mL).

2.9. Transfection to 293 Cells. The 293 cells were provided by the RIKEN Cell Line Bank (Japan) and were seeded on gelatin-coated 6-well culture plates (IWAKI, Tokyo, Japan). Cells were washed twice with 1 mL of Dulbecco's PBS(−) (Dainippon Pharmaceutical, Tokyo, Japan), and 1 mL of culture medium containing 10% FBS was then added to each well. A 100 μM amount of hydroxychloroquine was occasionally added in the transfection medium for the enhancement of gene expression.[34] Commercial LipofectAMINE reagent was used as a control gene vector. LipofectAMINE reagent (15 μL) was added to 100 μL of a pDNA solution (50 μg/mL) in 10 mM Tris-HCl buffer (pH 7.4) to form the lipoplex, and finally, the DNA concentration in the lipoplex solution was adjusted to 30 μg of pDNA/mL. A 100 μL volume of PIC micelle or lipoplex solution was applied to each well with 3 μg of pDNA/well. After 4 h of incubation, the medium was removed and replaced by fresh DMEM containing 10% FBS. After an additional 24 h of incubation, the cells were washed twice with 1 mL of PBS(−) and harvested in 100 μL of Promega cell lysis solution. After 10 min of incubation at room temperature, the lysate was centrifuged for 5 min at 13 000g at 25 °C. The luciferase activity of the lysate was measured using Fluoroskan Ascent FL (Thermo Labsystems, Finland) after the automatic injection of 100 μL of the assay buffer containing luciferin (Promega). Protein concentration in the cell lysate was measured using a Micro BCA Protein Assay Reagent Kit (Pierce) with bovine serum albumin as a standard.

2.10. Cytotoxicity of Acetal-PEG-PAMA/pDNA Micelles and PAMA/pDNA Polyplexes against 293 Cells. The 293 cells (1.5×10^4 cells/well) were seeded on gelatin-coated 96-well culture plates (IWAKI). After 24 h of incubation, the cultured cells were washed with the medium without FBS, and then 100 μL of culture medium containing 10% FBS and 100 μM hydroxychloroquine (hc) was added to each

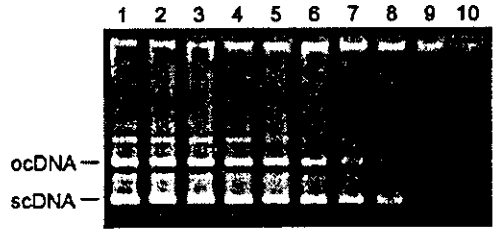

Figure 1. Gel retardation assay of acetal-PEG-PAMA/pDNA complexes. Samples were electrophoresed through 0.6% agarose gel under 2.8 V/cm: (lane 1) pDNA alone; (lanes 2−10) acetal-PEG-PAMA/pDNA complexes with progressively increasing N/P ratio (0.125, 0.25, 0.375, 0.5, 0.625, 0.75, 0.875, 1.0, 1.125). scDNA and ocDNA represent supercoiled DNA and open-circular DNA, respectively.

well. A 10 μL volume of PIC micelle or polyplex solution with various N/P ratios was added to each well with 0.3 μg of pDNA/well. In this assay, 10 mM Tris-HCl buffer (pH 7.4) and 2.2% Tween20 buffer solution were used as the negative and positive control, respectively. A 10 μL volume of control solution was also added to each well similarly to the complex solution. After 4 h of incubation at 37 °C in a CO_2 incubator, the released LDH activity of the cultured medium from each well was measured according to the manufacturer's protocol for a LDH-cytotoxic test kit (Wako Pure Chemical). The cytotoxicity of the PIC micelle and polyplex was quantified in the terms of the percentage of LDH release, which was calculated as follows:

$$\%\ \text{LDH release} = \frac{(\text{LDH}_{\text{complex}} - \text{LDH}_{\text{buffer}})}{(\text{LDH}_{2.2\%\text{Tween20}} - \text{LDH}_{\text{buffer}})} \times 100$$

Here $\text{LDH}_{\text{complex}}$, $\text{LDH}_{\text{buffer}}$, and $\text{LDH}_{2.2\%\text{Tween20}}$ represent the released LDH activity of the PIC micelle or polyplex, the buffer, and 2.2% Tween20, respectively. The results were expressed as the mean ± SEM; $n = 8$.

3. Results and Discussion

3.1. Gel Retardation Assay. PIC micelles were prepared by simple and direct mixing of pDNA and acetal-PEG-PAMA solutions at various residual molar mixing ratios (N/P ratio). The micelle solutions remained transparent over a long-time storage, and no precipitation was observed over the entire range of N/P ratios examined. To demonstrate the complex formation between acetal-PEG-PAMA and pDNA, a gel retardation assay was performed by electrophoresis of the pDNA/acetal-PEG-PAMA mixture on 0.6 w/w % agarose gel. With an increase in the N/P ratio, the amount of migrating free pDNA gradually decreased, indicating the polyion complex formation of pDNA with acetal-PEG-PAMA (Figure 1). Complete retardation of pDNA was accomplished at N/P = 1. It was determined from acid−base titration that the pK_a value of the acetal-PEG-PAMA used in this study is 7.1. Thus, the calculated neutralizing point from this pK_a value should be N/P = 2.5. Deviation of the experimental value from the calculated one may be ascribed to the facilitated protonation of AMA units in the process of complexation with pDNA. It should be noted that, in the formation of the polyion complex between a pair of

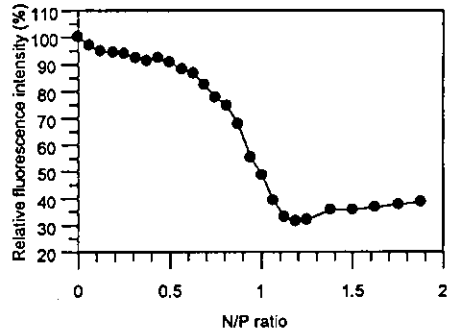

Figure 2. Estimation of pDNA condensation by acetal-PEG-PAMA. Samples were prepared at various N/P ratios in 10 mM Tris-HCl buffer (pH 7.4). The concentrations of pDNA and ethidium bromide (EtBr) were 20 and 0.4 μg/mL, respectively. All measurements were performed at 25.0 ± 0.2 °C (λ_{ex} = 510 nm, λ_{em} = 590 nm). Results are represented as relative fluorescence intensity (%) at each N/P ratio.

weak and strong polyelectrolytes, ionization of the weak polyelectrolyte is generally induced.[35,36] This is because a neighboring group facilitates the neutralization between a pair of oppositely charged groups, allowing the complex to have increased stability through the reduced electrostatic repulsion and the counterion release from the microenvironment.

3.2. Ethidium Bromide Exclusion Assay. Ethidium bromide (EtBr) is known to form an intercalating complex with double helical polynucleotides to show a striking enhancement in its fluorescence intensity.[37] However, the complex formation between DNA and a cationer results in quenching of the fluorescence, because charge neutralization and subsequent condensation of DNA prevents EtBr from intercalating into DNA. This characteristic of EtBr is frequently utilized to estimate the degree of pDNA condensation through complexation with a cationic polymer.[11,17] As shown in Figure 2, the fluorescence intensity of EtBr decreased with an increase in the N/P ratio and reached a minimum (approximately 30% of the initial value) around N/P = 1.2. This decreased fluorescence is consistent with the progressive complexation of acetal-PEG-PAMA with pDNA, inhibiting the intercalation of EtBr into pDNA. Of interest was the observation of a region which showed a steep decrease in the fluorescence (N/P = 0.7 to 1.2). To understand this characteristic change in fluorescence intensity from the viewpoint of the conformational change of pDNA, it is worth referring to DNA condensation as a DNA conformational change between the elongated coil and condensed globular states. Recently, a series of direct observation studies using fluorescence microscopy revealed that single, long duplex DNAs (T4 phage DNA) exhibit a large discrete coil−globule transition induced by the addition of polycations.[38] Although a direct observation of this transition in a much smaller pGL3-Luc plasmid DNA under optical microscopy has an inherent difficulty, it is reasonable to assume that the quenched fluorescence observed at N/P > 0.7 may be attributed to the coil-to-globule transition of pDNA in a manner similar to that observed in T4 phage DNA. Note that the apparent end point of the coil-to-globule transition (N/P ~ 1.2), assessed from EtBr exclusion, was consistent with the results of the gel retardation assay seen

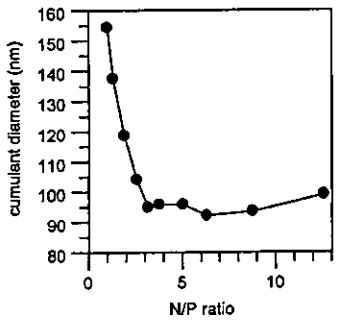

Figure 3. Change in the cumulant diameter with the N/P ratio for polyion complex micelles prepared from acetal-PEG-PAMA and pDNA. Dynamic light scattering (DLS) measurements were carried out at 25.0 ± 0.2 °C for 30 μg/mL of pDNA in 10 mM Tris-HCl buffer (pH 7.4).

in Figure 1, in which the vanishing point of the free pDNA band is N/P ~ 1.0.

3.3. Dynamic Light Scattering Measurements. On the basis of the results of gel retardation as well as EtBr exclusion assays, it is safe to assume that, in the region of N/P ≥ 1.0, pDNA in the solution is essentially complexed with acetal-PEG-PAMA to form a condensed structure. To gain insight into the size of these complexes, dynamic light scattering (DLS) measurements were then performed at various N/P ratios higher than unity. As seen in Figure 3, cumulant analysis of DLS data revealed the formation of pDNA-entrapped micelles whose sizes are around 155 nm at N/P = 1.0, followed by a steep decrease in the size with increased N/P ratio. The diameter of the micelle leveled off to approximately 95 nm around the N/P ratio of 3. The small size of the PIC micelles compared to the dimensions of free pDNA is consistent with the results of the EtBr exclusion assay, indicating the effective condensation of complexed pDNA.

It was suggested from the EtBr exclusion assay that pDNA would be in a fully condensed state already around N/P = 1.2. Thus, a significant diameter reduction in the region of N/P 1.0−3.0 would not be solely ascribed to the condensation of pDNA. Presumably, similar to the previously reported case of a PIC micelle formed from PEG-PLL and pDNA,[17] there may be a reduction in the association number to form nonstoichiometric micelles. Note that static light scattering (SLS) measurements revealed that nonstoichiometric micelles from PEG-PLL/pDNA were composed of only a single molecule of pDNA associated with approximately 150 strands of PEG-PLL (single pDNA complex).[17] The appreciably small size (~95 nm) of the acetal-PEG-PAMA/pDNA micelle comparable to that from PEG-PLL/pDNA is suggestive of the formation of a single pDNA complex, yet detailed SLS measurements may be needed to confirm the complex structure. Formation of a nonstoichiometric complex in the region of N/P ≥ 1 is presumably due to the steric restraint of supercoiled pDNA, requiring excess PAMA strands to participate in the ion-pair formation with residual phosphate groups in the pDNA strands to promote further condensation. Eventually, an increased PEG content in the micelles with an increased N/P prevents pDNA from a secondary coalescence to reduce the association number.[17]

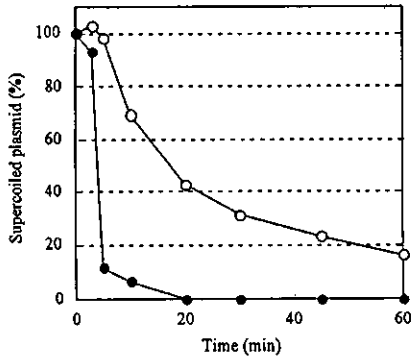

Figure 4. Stability of supercoiled pDNA complexed with acetal-PEG-PAMA against DNase I. Free pDNA (●) and acetal-PEG-PAMA/pDNA micelle (N/P = 1) (○) were treated with DNase I at 37 °C. After a defined time, the remaining supercoiled pDNA was quantified by the fluorescence imager following the gel electrophoresis.

3.4. Stability of pDNA Complexed with Acetal-PEG-PAMA against DNase I. The protection of the loaded pDNA from degradation by nuclease is an important requisite for gene delivery systems used in vivo. In this study, acetal-PEG-PAMA/pDNA micelles were treated with DNase I, followed by detection of the intact supercoiled pDNA by gel electrophoresis. The percentage of the remaining supercoiled pDNA, which was quantified by fluorescence densitometry, was shown in Figure 4. The naked pDNA was completely degraded within 20 min. In contrast, acetal-PEG-PAMA/pDNA micelles showed 43% of the remaining supercoiled pDNA even after 20 min of the nuclease treatment. Thus, the nuclease resistance of supercoiled pDNA was appreciably improved by the micelle formation with acetal-PEG-PAMA. The characteristic structure of acetal-PEG-PAMA/pDNA micelles, where the stable PIC core entrapping pDNA is surrounded by the PEG palisade, might restrict the approach of nuclease to pDNA, resulting in an increased nuclease resistance.

3.5. Stability of Acetal-PEG-PAMA/pDNA Micelles and PAMA/pDNA Polyplexes in the Exchange Reaction with Polyanions. Gene vector systems should stably incorporate pDNA capable of tolerating the cellular uptake process as well as being protective against nuclease attack. On the other hand, inside the target cells, gene vectors need to release the loaded pDNA for transcription. It is believed that an exchange reaction with negatively charged biomacromolecules in a biological environment would be a major mechanism of pDNA release from polyplex systems.[14] In this regard, the exchange assay of complexed pDNA with model polyanion compounds is of appreciable importance to estimate the stability of the polyplexes.

The release of pDNA from acetal-PEG-PAMA/pDNA micelles and PAMA/pDNA polyplexes due to the exchange reaction with PVSK as a model polyanion was evaluated through agarose gel electrophoresis at physiological pH (pH 7.4). As shown in Figure 5a, in acetal-PEG-PAMA/pDNA micelles, released pDNA (supercoiled DNA (scDNA) and open-circular DNA (ocDNA)) were clearly observed as discrete bands for the PVSK-added sample with N/P = 1.25. On the other hand, the intensities of bands corresponding to scDNA and ocDNA became scattered for the system with

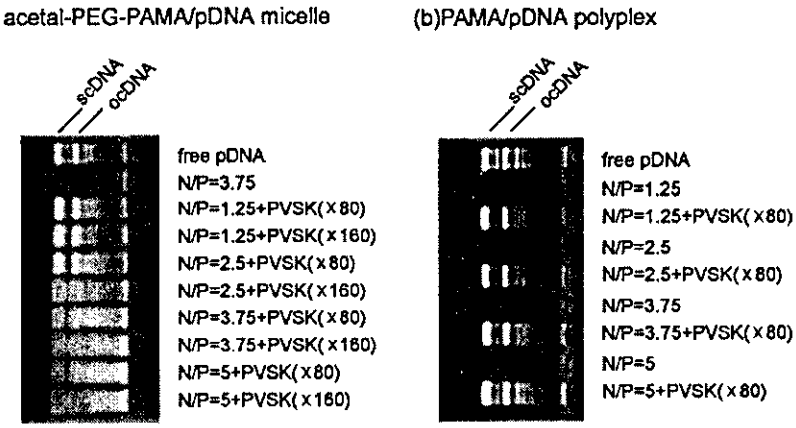

Figure 5. Stability of acetal-PEG-PAMA/pDNA micelle (a) and PAMA/pDNA polyplex (b) toward exchange reaction with polyanions. Acetal-PEG-PAMA/pDNA micelle and PAMA/pDNA polyplex were prepared at various N/P ratios (N/P = 1.25, 2.5, 3.75, 5) in 10 mM Tris-HCl buffer (pH 7.4), respectively. (a) acetal-PEG-PAMA/pDNA micelle: 80 or 160 equiv of poly(vinyl sulfate) (PVSK)/AMA unit of acetal-PEG-PAMA was added to the acetal-PEG-PAMA/pDNA micelle. After incubation at room temperature overnight, samples were electrophoresed through 0.6% agarose gel in buffer (pH 7.4, 3.3 mM Tris-AcOH + 1.7 mM AcONa + 1 mM EDTA2Na). (b) PAMA/pDNA polyplex: 80 equiv of PVSK/nucleotide of pDNA was added to the PAMA/pDNA polyplex. After incubation at room temperature overnight, samples were electrophoresed in the same way.

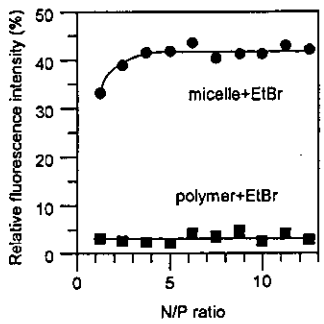

Figure 6. Fluorescence intensity of EtBr in the presence of acetal-PEG-PAMA/pDNA micelles with different N/P ratios (N/P = 1.25–12.5) and acetal-PEG-PAMA block copolymers alone with the corresponding concentrations. Fluorescence measurements were performed as described in the Experimental Section (2.4. Ethidium Bromide Exclusion Assay). Key: ●, acetal-PEG-PAMA/pDNA micelle; ■, acetal-PEG-PAMA block copolymers alone. Results are represented as a value relative to the fluorescence intensity of pDNA solution without acetal-PEG-PAMA (N/P = 0).

N/P = 2.5 and were finally smeared at an N/P higher than 3.75. This result demonstrates that acetal-PEG-PAMA still interacts with pDNA even in the presence of excess PVSK, suggesting a substantial contribution of a stabilizing factor other than simple electrostatic interaction for pDNA association with acetal-PEG-PAMA. It should be noted that, in the EtBr exclusion assay, the relative fluorescence intensity slightly increased above an N/P of 1.2 (Figure 2). This result is likely to suggest a change in the microenvironment around condensed pDNA. Indeed, a further increase in the N/P ratio as seen in Figure 6 results in appreciable recovery of the relative fluorescence intensity to approximately 40% of the initial value, leveling off at around an N/P of 3–4. Note that there was no change in the fluorescence intensity of the mixed solution of EtBr and acetal-PEG-PAMA, which remained at a very low value, regardless of an increase in the polymer concentration. Thus, EtBr association with PIC micelles having excess acetal-PEG-PAMA is responsible for this enhancement in the fluorescence intensity. It is reasonable to assume that, in nonstoichiometric PIC micelles, a portion of the deprotonated amino groups in the PAMA segments may increase with an increase in the N/P ratio. Presumably, the presence of nonprotonated tertiary amine in the PIC micelle with a higher N/P value may enhance the hydrophobicity of the microenvironment within a complexed pDNA, allowing the PIC to be stabilized through decreased local permittivity. It should be noted that the fluorescence quantum yield of EtBr increases in hydrophobic surroundings,[39] in line with a rebound in fluorescence intensity of EtBr in a PIC micelle system with N/P ≥ 1.

On the other hand, in PAMA/pDNA polyplexes, released pDNA was clearly observed at all N/P ratios at pH 7.4 (Figure 5b). This result is consistent with that reported by Heninnk et al.[40] From Figure 5a,b, it may be safe to conclude that acetal-PEG-PAMA/pDNA micelles are more tolerant toward polyanion exchange than PAMA/pDNA polyplexes. This result suggests that the presence of the PEG layer would also contribute to increased affinity of the PAMA segment for pDNA in the complex. Indeed, our previous study revealed that block copolymerization of a polycation with PEG produced increased thermal stability of the complex with DNA compared to the polycation alone.[14] This unique behavior was explained to be due to an increase in the local concentration of PEG around complexed DNA to decrease the permittivity of the microenvironment. The stability of polycation/pDNA complexes under physiological condition is one of the important parameters that influence the transfection efficiency of polyplex type gene vectors.[40,41] In this regard, the enhanced stability of the block copolymer micelles compared to the homopolymer polyplexes at a physiological pH of 7.4 is a promising feature. Particularly worth noting about the acetal-PEG-PAMA/pDNA micelles is the increased local concentration of the PEG shell layer as well as the appreciably hydrophobic nature of the nonprotonated AMA units within the complexed pDNA, both substantially contributing to increased micelle stability under physiological condition.

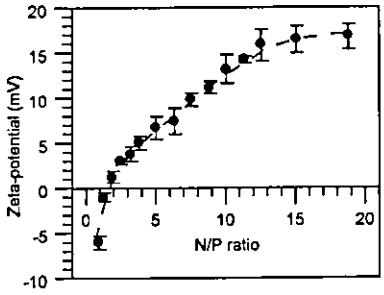

Figure 7. Change in ζ-potential with the N/P ratio for polyion complex micelle formed from pDNA and acetal-PEG-PAMA. ζ-potential measurements were carried out at 25.0 ± 0.2 °C for 30 μg/mL of pDNA in 10 mM Tris-HCl buffer (pH 7.4). Results are represented as the mean ± SD in triplicate.

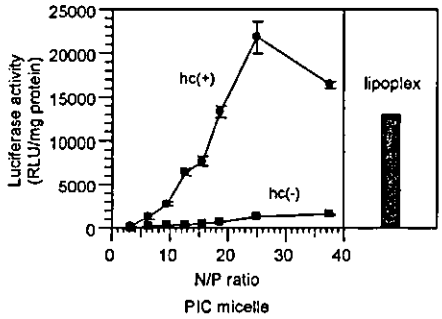

Figure 8. Effect of the N/P ratio of the acetal-PEG-PAMA/pDNA micelles on transfection efficiency toward 293 cells. The cells were transfected with acetal-PEG-PAMA/pDNA micelle for 4 h in the transfection medium containing 10% FBS in the presence or absence of 100 μM hydroxychloroquine (hc). Results are represented as the mean ± SEM in triplicate.

3.6. ζ-Potential Measurement. ζ-potential measurement was then carried out for PIC micelles with varying N/P ratios to explore their surface electrostatic properties. Although the results of DLS and the EtBr exclusion assay indicate that, in the region with N/P ≥ 4, the micelles seem to have an almost constant size of ca. 95 nm with the core composed of fully condensed pDNA, an appreciable increase in the ζ-potential even in this region was still observed as seen in Figure 7. This increase in ζ-potential finally leveled off at around N/P = 15, becoming a value of approximately 15 mV. Note that this value corresponds to about 1/2 of the value observed for a polyplex between a PAMA homopolymer and pDNA.[25,26] Presumably, excess PEG-PAMA chains may loosely associate on the surface of the micelles in the region of 4 ≤ N/P ≤ 15 to cause a substantially positive ζ-potential. Although the driving force of this unusual association of excess block copolymers on the micelles under a condition highly deviating from the charge-stoichiometric point is still unclear, a similar phenomenon was occasionally observed in the PIC micelle formation from a pair of a block ionomer and oppositely charged polyelectrolytes, including proteins.[42]

3.7. Transfection to 293 Cells. To gain insight into the relationship between the transfection potential of acetal-PEG-PAMA/pDNA micelles and their aforementioned physicochemical properties, a transfection experiment was performed with 293 cells using the micelles prepared at various N/P ratios. Note that transfection was carried out in the medium with and without hydroxychloroquine. Hydroxychloroquine is a derivative of chloroquine, a well-known lysosomotropic reagent, yet it has approval for use in clinics for the treatment of rheumatoid arthritis and lupus erythematosus.[34]

The results of both the DLS measurement and the EtBr exclusion assay suggest that the micelle seems to reach a state of constant size and microenvironment at an N/P ratio of 3−4. Nevertheless, effective gene expression was not observed in this N/P range even in the presence of 100 μM hydroxychloroquine. Worth noting is an appreciable increase in the transfection efficiency in the region of N/P ≥ 4 as seen in Figure 8. Luciferase activity reached a maximum at N/P = 25 and was even higher than that achieved by a lipoplex under the same conditions except for the absence of hydroxychloroquine. This increased trend in gene expression with the N/P ratio is obviously correlated to the increment in ζ-potential of the micelles as seen in Figure 7. Presumably, cationization of the micelles may facilitate their association with the cellular surface, improving the internalized efficiency into the intracellular compartment. It should be noted that the transfection revealed a further stepwise increase even in the region of N/P ≥ 15, where the cationization process of the micelles becomes saturated judging from the ζ-potential measurements. This increment in transfection at N/P ≥ 15 is most likely due to the involvement of excess block copolymers existing in free form in the medium. Approximately 40% of the amino groups in the PAMA segment of the free block copolymer are calculated to be in nonprotonated form at pH 7.4 on the basis of the pK_a = 7.1 of PEG-PAMA. Thus, free PEG-PAMA, if any exists in the system, is expected to show a proton sponge effect after its possible transport into the endosome. Note that Hennink et al. indeed observed the proton sponge effect of PAMA,[25,26] yet the efficacy was lower than that of poly(ethylenimine), requiring chloroquine as an adjuvant for appreciably high gene expression.[26] This is in line with our results using the acetal-PEG-PAMA block copolymer, showing a definite and steep enhancement of gene expression in the presence of hydroxychloroquine. The transfection efficiency of PIC micelles reached a maximum at N/P = 25. Further increase in the N/P ratio to 37.5 results in decreased efficiency probably due to the cytotoxicity of free acetal-PEG-PAMA in the system as will be described in the following paragraph.

The cytotoxicity of PIC micelles was evaluated by LDH assay in the transfection medium containing 10% FBS and 100 μM hydroxychloroquine, and the results are summarized in Table 1. An LDH assay was used here because damage to the plasma membrane is believed to be the main toxicity of the polycation interacting with a negatively charged cell surface.[43] Results for the PAMA/pDNA polyplex as control are also shown in the table. Notably, LDH release was almost negligible for both the PIC micelle and the PAMA/pDNA polyplex in the region of N/P ≤ 15. There was a slight increase in LDH release up to 15% in the region of N/P ≥ 15 probably due to the membrane toxicity of free polymers in the medium.

It is worth mentioning that nonstoichiometric micelles with a positively charged character (ζ-potential = 15 mV)

Table 1. Cytotoxic Effect of Acetal-PEG-PAMA/PDNA Micelles and PAMA/PDNA Polyplexes on 293 Cells[a]

	cytotoxicity (% LDH release)	
N/P ratio	PAMA/pDNA polyplex	acetal-PEG-PAMA/pDNA micelle
5	1.93 ± 0.46	0.44 ± 0.35
10	0.22 ± 0.47	0.87 ± 0.60
15	2.53 ± 0.77	2.32 ± 0.82
25	3.13 ± 0.71	10.45 ± 1.04
37.5	5.81 ± 0.78	13.62 ± 1.22

[a] Acetal-PEG-PAMA/pDNA micelles and PAMA/pDNA polyplexes were prepared at various N/P ratios in 10 mM Tris-HCl buffer (pH 7.4). Each sample solution was added to each well with 293 cells cultured in a medium containing 10% FBS and 100 μM hydroxychloroquine. After 4 h of incubation at 37 °C, cytotoxicity was estimated by LDH assay. Results are represented as the mean ± SEM of eight determinations.

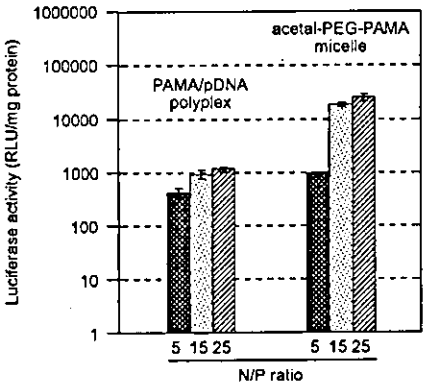

Figure 9. Comparison of acetal-PEG-PAMA/pDNA micelles with PAMA/pDNA polyplexes on transfection efficiency toward 293 cells. The cells were transfected with each pDNA complex for 4 h in transfection medium containing 10% FBS in the presence of 100 μM hydroxychloroquine (hc). Results are represented as the mean ± SEM in triplicate.

prepared at N/P = 15 had negligibly low cytotoxicity yet maintained considerable transfection efficiency. As seen in Figure 9, the acetal-PEG-PAMA/pDNA micelle showed approximately 1 order of magnitude higher transfection efficiency than the PAMA/pDNA polyplex at N/P = 15. This improved transfection efficiency of the micelle system compared to the homopolymer polyplex system is consistent with the increased stability of the former in comparison with the latter evaluated from the polyanion displacement assay demonstrated in Figure 5. It may be reasonable to assume that improved stability of the pDNA complex is a merit for increased pDNA transport into the intracellular compartment as well as for the protection of pDNA from harsh environmental conditions.

4. Conclusions

In this study, the PIC micelle formed from the acetal-PEG-PAMA block copolymer and pDNA was investigated with regard to the possibility as a novel gene vector. Through the EtBr exclusion assay and the dynamic light scattering measurements, it was demonstrated that the acetal-PEG-PAMA effectively induced the condensation of pDNA to be incorporated into PIC micelle having approximately 90–100 nm of diameter. PEG segments of the block copolymer are likely to surround the condensed pDNA to ensure the colloidal stability of the PIC micelles. Indeed, the PIC micelles showed greatly improved nuclease resistance of the loaded pDNA. Also, stabilization of the PIC micelle compared to that of the PAMA/pDNA polyplex was demonstrated from the exchange reaction of complexed pDNA with counterpolyanion (PVSK). In addition, DNA release from the PIC micelle induced by PVSK was dependent on an N/P ratio, suggesting that the presence of nonprotonated tertiary amines may contribute to the increased stability of the complex presumably through the formation of hydrophobic microenvironment. It should be noted that a more detailed study on the interaction of the PIC micelles with biological components, including blood cells and serum proteins, is indispensable to verify the utility of the micelle systems as in vivo gene carrier systems particularly injectable through intra venous route. The acetal-PEG-PAMA/pDNA micelles prepared at a highly deviated N/P ratio of 15 have a positively charged character, presumably due to the loose association of excess PEG-PAMA into the micelle, and achieved an appreciably higher gene expression than that observed in the PAMA/pDNA without any significant cytotoxicity in the presence of 10% serum and 100 μM hydorxychloroquin.

Furthermore, an acetal moiety on the micelle can be easily converted into the reactive aldehyde group, which is available to install various ligands useful for the receptor-mediated targeting of the micelles. The research in this direction is now underway in our laboratory, and results will be reported elsewhere.[31]

Acknowledgment. This work was financially supported by the Special Coordination Funds for Promoting Science and Technology as well as a Grant for the 21st Century COE Program "Human-Friendly Materials Based on Chemistry" from the Ministry of Education, Science, Sports, Science, and Technology of Japan and by the Core Research Program for Evolutional Science and Technology (CREST) from the Japan Science and Technology Corp. (JST).

References and Notes

(1) Roemer, K.; Friedmann, T. *Eur. J. Biochem.* **1992**, *208*, 211–215.
(2) Miller, A. D. *Nature* **1992**, *357*, 455–460.
(3) Mulligan, R. C. *Science* **1993**, *260*, 926–932.
(4) Morgan, R. A.; Anderson, W. F. *Annu. Rev. Biochem.* **1993**, *62*, 191–217.
(5) Gao, X.; Huang, L. *Gene Ther.* **1995**, *2*, 710–722.
(6) Kabanov, A. V.; Astafieva, I. V.; Maksimova, I. V.; Lukanidin, E. M.; Georgiev, G. P.; Kabanov, V. A. *Bioconjug. Chem.* **1993**, *4*, 448–454.
(7) Wu, G. Y.; Wu, C. H. *J. Biol. Chem.* **1988**, *263*, 14621–14624.
(8) De Smedt, S. C.; Demeester, J.; Hennink, W. E. *Pharm. Res.* **2000**, *17*, 113–126.
(9) Kabanov, A. V.; Kabanov, V. A. *Bioconjug. Chem.* **1995**, *6*, 7–20.
(10) Pouton, C. W.; Lucas, P.; Thomas, B. J.; Uduehi, A. N.; Milroy, D. A.; Moss, S. H. *J. Controlled Release* **1998**, *53*, 289–299.
(11) Choi, Y. H.; Liu, F.; Kim, J. S.; Choi, Y. K.; Park, J. S.; Kim, S. W. *J. Controlled Release* **1998**, *54*, 39–48.
(12) Wolfert, M. A.; Schacht, E. H.; Toncheva, V.; Ulbrich, K.; Nazarova, O.; Seymour, L. W. *Hum. Gene Ther.* **1996**, *7*, 2123–2133.
(13) Kabanov, A. V.; Vinogradov, S. V.; Suzdaltseva, Y. G.; Alakhov, V. Y. *Bioconjug. Chem.* **1995**, *6*, 639–643.
(14) Katayose, S.; Kataoka, K. *Bioconjug. Chem.* **1997**, *8*, 702–707.
(15) Katayose, S.; Kataoka, K. *J. Pharm. Sci.* **1998**, *87*, 160–163.
(16) Itaka, K.; Harada, A.; Nakamura, K.; Kawaguchi, H.; Kataoka, K. *Biomacromolecules* **2002**, *3*, 841–845.

(17) Itaka, K.; Yamauchi, K.; Harada, A.; Nakamura, K.; Kawaguchi, H.; Kataoka, K. *Biomaterials* **2003**, *24*, 4495−4506.
(18) Harada-Shiba, M.; Yamauchi, K.; Harada, A.; Takamisawa, I.; Shimokado, K.; Kataoka, K. *Gene Ther.* **2002**, *9*, 402−414.
(19) Ogris, M.; Brunner, S.; Schuller, S.; Kircheis, R.; Wagner, E. *Gene Ther.* **1999**, *6*, 595−605.
(20) Ward, C. M.; Pechar, M.; Oupicky, D.; Ulbrich, K.; Seymour, L. W. *J. Gene Med.* **2002**, *4*, 536−547.
(21) van de Wetering, P.; Moret, E. E.; Schuurmans-Nieuwenbroek, N. M. E.; van Steenbergen, M. J.; Hennink, W. E. *Bioconjug. Chem.* **1999**, *10*, 589−597.
(22) Takai, T.; Ohmori, H. *Biochim. Biophys. Acta* **1990**, *1048*, 105−109.
(23) Zauner, W.; Ogris, M.; Wagner, E. *Adv. Drug Delivery Rev.* **1998**, *30*, 97−113.
(24) Boussif, O.; Lezoualc'h, F.; Zanta, M. A.; Mergny, M. D.; Acherman, D.; Demeneix, B.; Behr, J. P. *Proc. Natl. Acad. Sci. U.S.A.* **1995**, *92*, 7297−7301.
(25) Cherng, J. Y.; van de Wetering, P.; Talsma, H.; Crommelin, D. J. A.; Hennink, W. E. *Pharm. Res.* **1996**, *13*, 1038−1042.
(26) van de Wetering, P.; Cherng, J. Y.; Talsma, H.; Hennink, W. E. *J. Controlled Release* **1997**, *49*, 59−69.
(27) MacLaughlin, F. C.; Mumper, R. J.; Wang, J.; Tagliaferri, F.; Gill, I.; Hinchcliffe, M.; Rolland, A. *J. Controlled Release* **1998**, *56*, 259−272.
(28) Wolfert, M. A.; Dash, P. R.; Nazarova, O.; Oupicky, D.; Seymour, L. W.; Smart, S.; Strohalm, J.; Ulbrich, K. *Bioconjug. Chem.* **1999**, *10*, 993−1004.
(29) van de Wetering, P.; Zuidam, N. J.; van Steenbergen, M. J.; van der Houwen, O. A. G. J.; Underberg, W. J. M.; Hennink, W. E. *Macromolecules* **1998**, *31*, 8063−8068.
(30) Kataoka, K.; Harada, A.; Wakebayashi, D.; Nagasaki, Y. *Macromolecules* **1999**, *32*, 6892−6894.
(31) Wakebayashi, D.; Nishiyama, N.; Yamasaki, Y.; Itaka, K.; Kanayama, N.; Harada, A.; Nagasaki, Y.; Kataoka, K. *J. Controlled Release* **2004**, *95*, 653−664.
(32) Nagasaki, Y.; Sato, Y.; Kato, M. *Macromol. Rapid Commun.* **1997**, *18*, 827−835.
(33) Harada, A.; Kataoka, K. *Macromolecules* **1995**, *28*, 5294−5299.
(34) Itaka, K.; Miyata, K.; Harada, A.; Kawaguchi, H.; Nakamura, K.; Kataoka, K. In *Carrier-Based Drug Delivery*; ACS Symposium Series; Svenson, S., Ed.; American Chemical Society: Washington, DC, in press.
(35) Abe, K.; Ohno, H.; Tsuchida, E. *Makromol. Chem.* **1977**, *178*, 2285−2293.
(36) Kabanov, A. V.; Bronich, T. K.; Kabanov, V. A.; Eisenberg, K. Yu, A. *Macromolecules* **1996**, *29*, 6797−6802.
(37) Lepecq, J.-B.; Paoletti, C. *J. Mol. Biol.* **1967**, *27*, 87−106.
(38) Yamasaki, Y.; Katayose, S.; Kataoka, K.; Yoshikawa, K. *Macromolecules* **2003**, *36*, 6276−6279.
(39) Pyun, C.-H.; Park, S.-M. *Bull. Korean Chem. Soc.* **1989**, *10*, 142−147.
(40) Arigita, C.; Zuidam, N. J.; Crommelin, D. J. A.; Hennink, W. E. *Pharm. Res.* **1999**, *16*, 1534−1541.
(41) Mullen, P. M.; Lollo, C. P.; Phan, Q.-C.; Amini, A.; Banaszczyk, M. G.; Fabrycki, J. M.; Wu, D.; Carlo, A. T.; Pezzoli, P.; Coffin, C. C.; Carlo, D. J. *Biochim. Biophys. Acta* **2000**, *1523*, 103−110.
(42) Harada, A.; Kataoka, K. *Langmuir* **1999**, *15*, 4208−4212.
(43) Choksakulnimitr, S.; Masuda, S.; Tokuda, H.; Takakura, Y.; Hashida, M. *J. Controlled Release* **1995**, *34*, 233−241.

BM040009J

J|A|C|S
COMMUNICATIONS

Published on Web 09/30/2004

Supramolecular Nanocarrier of siRNA from PEG-Based Block Catiomer Carrying Diamine Side Chain with Distinctive pK_a Directed To Enhance Intracellular Gene Silencing

Keiji Itaka,[†,‡] Naoki Kanayama,[†] Nobuhiro Nishiyama,[†] Woo-Dong Jang,[†] Yuichi Yamasaki,[†] Kozo Nakamura,[‡] Hiroshi Kawaguchi,[‡] and Kazunori Kataoka*[,†]

Department of Materials Science and Engineering, Graduate School of Engineering, and Department of Orthopaedic Surgery, Faculty of Medicine, University of Tokyo, 7-3-1 Hongo, Bunkyo-ku, Tokyo 113-8656, Japan

Received May 14, 2004; E-mail: kataoka@bmw.t.u-tokyo.ac.jp

The short double-stranded RNA species, called short interference RNA (siRNA), can be used to silence the gene expression in a sequence-specific manner in a process that is known as RNA interference (RNAi).[1] It has become a useful method for the analysis of gene functions and holds the significant possibility of therapeutic application. However, to promote an efficient gene knockdown, especially in an in vivo situation, two substantial issues must be considered: tolerability under physiological conditions and enhanced cellular uptake. Thus, the development of effective siRNA delivery systems is required.

Recently, a new delivery system of plasmid DNA and oligonucleotides has been developed, based on the micellar assembly of the poly-ion complex (PIC) of these compounds with block copolymers consisting of poly(ethylene glycol) (PEG) and polycation segments, leading to the self-assembled structure with a core−shell architecture (PIC micelles).[2] Their excellent properties for in vivo DNA delivery have been confirmed so far:[3] a diameter around 100 nm with a PEG palisade which enables complexes to avoid recognition by reticuloendothelial systems, increased nuclease resistance, increased tolerance under physiological conditions, and the excellent gene expression in a serum-containing medium.[4]

We now describe the structural design of a novel block catiomer-based PIC particularly available for siRNA delivery. PEG−poly(3-[(3-aminopropyl)amino]propylaspartamide (PEG-DPT; PEG, 12 000 g/mol, polymerization degree of DPT segment, 68), carrying a diamine side chain with distinctive pK_a, was newly synthesized by a side-chain aminolysis reaction of PEG−poly(β-benzyl-L-aspartate) block copolymer (PEG-PBLA) with dipropylene triamine (DPT) (Figure 1A and Figure S1 in the Supporting Information). A model compound of a DPT unit, *tert*-butoxycarbonyl-β-*N*-3-(3-aminopropyl)aminopropylamido-α-*N*-propyl-(L)-aspartamide (Boc-Asp(DPT)-Pr), was also synthesized (see Supporting Information) to determine the pK_a values of the amino groups.

Boc-Asp(DPT)-Pr clearly gave a two-stage pH−α curve (Figure 1B), from which the pK_a values of the primary and secondary amino groups were determined to be 9.9 and 6.4, respectively. Amino groups in the PIC of polyamine with polynucleotides including siRNA generally undergo facilitated protonation due to the zipper effect or the neighboring group effect during the complexation process, hampering the proton buffering or the proton sponge capacity. The unique feature of PEG-DPT is the regulated location of primary and secondary amino groups in the side chain: the former, with higher pK_a, settles at the distal end of the side chain to participate in the ion complex formation with phosphate groups in siRNA molecule, whereas the latter, with lower pK_a, located closer to the polymer backbone, is expected to leave a substantial

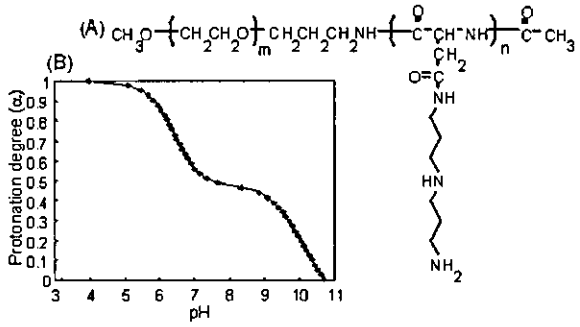

Figure 1. (A) Chemical structure of PEG-DPT. (B) Change in protonation degree (α) with pH for Boc-Asp(DPT)-Pr.

fraction of unprotonated form even in the complex, presumably due to the lower protonation power and the spatial restriction, directing to the enhanced intracellular activity of siRNA through the buffering capacity in the endosomal compartment.

The formation of the siRNA complex with the PEG-DPT was confirmed by polyacrylamide gel electrophoresis (PAGE) and the ethidium bromide (EtBr) exclusion assay (see Figure S2 in the Supporting Information). Note that intercalators such as EtBr bind the double-stranded (ds) RNA in the same fashion as dsDNA.[5] The free siRNA disappeared at the N/P ratio (= [total amines in cationic segment]/[siRNA phosphates]) >2, in line with a substantial fluorescence quenching of EtBr at N/P ≥ 2 due to the inaccessibility of EtBr to the complexed siRNA with PEG-DPT. Furthermore, the EtBr assay highlights the distinctive role of primary and secondary amino groups of the side chain in the complex. The PIC of the double-stranded oligo DNA, composed of sequences similar to the GL3 targeting siRNA, with PEG−poly(3-dimethylamino)propyl aspartamide (PEG-DMAPA; pK_a ≈ 7.9, see Figure S3 for chemical structure), revealed a lower degree of EtBr quenching compared to the PEG-DPT/ds-oligo DNA PIC, even in the region of excess N/P ratios (see Figure S4), suggesting that the presence of unprotonated amino groups in the former may hamper the tight association. PEG−poly(L-lysine) (PEG-PLL; pK_a ≈ 9.37, see Figure S3 for chemical structure) induced EtBr quenching as significantly as PEG-DPT upon complexation with the ds-oligo DNA, yet the quenching leveled off at the stoichiometric N/P ratio (N/P = 1.0) (Figure S4). This is in sharp contrast with the PEG-DPT/ds-oligo DNA complex, which showed leveling-off behavior of EtBr quenching at N/P ≈ 2.0, suggesting that secondary amines with the lower pK_a may be excluded from the ion complexation with oligonucleotides.

These distinctive features of the PEG-DPT, PEG-DMAPA, and PEG-PLL complexes indeed correlated with their gene knockdown abilities. For this evaluation, the GL3 luciferase gene was targeted

[†] Department of Materials Science and Engineering.
[‡] Department of Orthopaedic Surgery.

10.1021/ja047174r CCC: $27.50

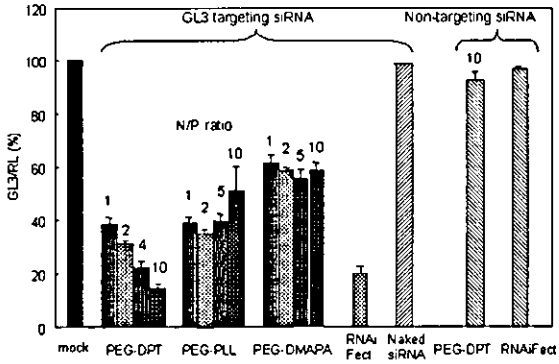

Figure 2. GL3 luciferase gene knockdown ($n = 4$; ±SD).

after transfecting two kinds of luciferase pDNAs (pGL3 and pRL; Promega) to HuH-7 cells. The expression ratio of GL3/RL was used as the knockdown marker.

Each complex system showed a sufficient knockdown of the GL3 luciferase, while neither the naked siRNA nor the nontargeting siRNA showed any knockdown (Figure 2). Thus, these results should be recognized as the veritable RNAi by the GL3-targeting siRNA delivered into the cytoplasm. Notably, the gene knockdown abilities of the siRNA/PEG-DPT complex were superior to those of the other two complexes, especially at higher N/P ratios. At N/P = 10, it showed more than an 80% knockdown, which exceeded the commercial RNAiFect. The cell viability evaluated by MTT assay was more than 75% of the mock cells, even after co-incubation with siRNA/PEG-DPT with N/P ≥ 10 (see Figure S5), suggesting the toxic effect to be eliminated. The siRNA/PEG-DMAPA complexes showed knockdown abilities to a lesser extent. Apparently, the loosely associated nature of siRNA, suggested by the EtBr exclusion assay, is unfavorable for facilitating an effective intracellular delivery of intact siRNA. PEG-PLL showed a considerable knockdown ability in the low N/P region, yet no particular enhancement with the increase in the N/P ratios. High efficacy of PEG-DPT may be characterized by the existence of additional secondary amines with a lower pK_a to promote the internalization of the siRNA molecules into the cytoplasm through buffering of the endosomal cavity, as is the case with the polyethylenimine-based polyplex that shows an enhanced tranfection efficiency at the higher N/P ratios.[6]

A serum incubation study was then performed to evaluate the complex stability under physiological conditions by incubating the complexes in 50% serum at 37 °C prior to transfection. The siRNA/PEG-DPT complexes showed comparable abilities of gene knockdown, even after co-incubation with serum for 30 min (Figure 3A). In contrast, the lipid-based RNAiFect system was significantly influenced by the serum incubation, probably due to the nonspecific association with serum proteins. Thus, these results highlighted the excellent feasibility of the PEG-DPT/siRNA complex, particularly under physiological conditions due to the segregation of siRNA into the PEG microenvironment.

The results of the endogenous gene knockdown were more fascinating. For this purpose, a cytoskeletal protein, Lamin A/C, was targeted.[1] The PEG-DPT system showed a significant gene knockdown of Lamin A/C mRNA, even after a 30-min preincubation in 50% serum, evaluated by the real-time RT-PCR analysis. Notably, in 293T cells, the expression was suppressed to the level of 20% of mock samples, which significantly exceeded the ability

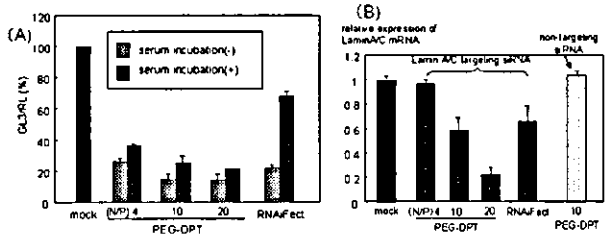

Figure 3. (A) GL3 knockdown by siRNA complexes after serum co-incubation with serum. (B) Endogenous gene (Lamin A/C) knockdown after co-incubation ($n = 4$; ±SD).

of the RNAiFect (Figure 3B). A similar trend was also observed in HuH-7 cells. However, neither the PEG-PLL nor PEG-DMAPA system showed any gene knockdown (data not shown). As Lamin A/C is assumed to abundantly express inside the cells, the threshold level of the siRNA's introduction that is necessary to show the inhibition of gene expression should be significantly higher than in the case of the luciferase cotransfection study. Thus, these results of PEG-DPT were very encouraging for the actual therapeutic knockdown of an endogenous gene by the siRNA delivering approach.

In conclusion, we reported here an effective siRNA nanocarrier system based on the self-assembly of the PEG-based block catiomer. The distinctive polymer design managed both a sufficient siRNA complexation and a buffering capacity of the endosomes. Notably, the siRNA/block catiomer complex revealed remarkable knockdown of the endogenous gene, even after the serum incubation. These results directed this newly designed system of block catiomer to have a promising feasibility for in vivo therapeutics.

Acknowledgment. This work was financially supported by the Core Research Program for Evolutional Science and Technology (CREST) from the Japan Science and Technology Corporation (JST) as well as by Special Coordination Funds for Promoting Science and Technology from the Ministry of Education, Culture, Sports, Science and Technology of Japan (MEXT).

Supporting Information Available: Detailed Materials and Methods section; ^{1}H NMR spectrum of PEG-DPT block copolymer (Figure S1); results of PAGE and EtBr exclusion assay of PEG-DPT (Figure S2); chemical structures of PEG-DMAPA and PEG-PLL (Figure S3); summary of EtBr exclusion assay of these copolymers (Figure S4); and result of MTT assay (Figure S5). This material is available free of charge via the Internet at http://pubs.acs.org.

References

(1) Elbashir, S. M.; Harborth, J.; Lendeckel, W.; Yalcin, A.; Weber, K.; Tuschl, T. *Nature* **2001**, *411*, 494−498.
(2) (a) Kataoka, K.; Togawa, H.; Harada, A.; Yasugi, K.; Matsumoto, T.; Katayose, S. *Macromolecules* **1996**, *29*, 8556−8557. (b) Katayose, S.; Kataoka, K. *Bioconjugate Chem.* **1997**, *8*, 702−707. (c) Vinogradov, S. V.; Bronich, T. K.; Kabanov, A. V. *Bioconjugate Chem.* **1998**, *9*, 805−812. (d) Choi, Y. H.; Liu, F.; Kim, J. S.; Choi, Y. K.; Park, J. S.; Kim, S. W. *J. Controlled Release* **1998**, *54*, 39−48. (e) Ogris, M.; Brunner, S.; Schuller, S.; Kircheis, R.; Wagner, E. *Gene Ther.* **1999**, *6*, 595−605. (f) Oupicky, D.; Konak, C.; Ulbrich, K.; Wolfert, M. A.; Seymour, L. W. *J. Controlled Release* **2000**, *65*, 149−171.
(3) Harada-Shiba, M.; Yamauchi, K.; Harada, A.; Takamisawa, I.; Shimokado, K.; Kataoka, K. *Gene Ther.* **2002**, *9*, 407−414.
(4) Itaka, K.; Yamauchi, K.; Harada, A.; Nakamura, K.; Kawaguchi, H.; Kataoka, K. *Biomaterials* **2003**, *24*, 4495−4506.
(5) Carlson, C.; Beal, P. A. *Biopolymers* **2003**, *70*, 86−102.
(6) Boussif, O.; Lezoualc'h, F.; Zanta, M. A.; Mergny, M. D.; Scherman, D.; Demeneix, B.; Behr, J. P. *Proc. Natl. Acad. Sci. U.S.A.* **1995**, *92*, 7297−7301.

JA047174R

Available online at www.sciencedirect.com

SCIENCE DIRECT®

Journal of Controlled Release 97 (2004) 345–356

journal of controlled release

www.elsevier.com/locate/jconrel

Block copolymer-coated calcium phosphate nanoparticles sensing intracellular environment for oligodeoxynucleotide and siRNA delivery

Yoshinori Kakizawa[a], Sanae Furukawa[a], Kazunori Kataoka[a,b,*]

[a] *Biomaterials Center, National Institute for Materials Science, 1-1 Namiki, Tsukuba, Ibaraki 305-0044, Japan*
[b] *Department of Materials Science, Graduate School of Engineering, The University of Tokyo, 7-3-1 Hongo, Bunkyo, Tokyo 113-8656, Japan*

Received 22 November 2003; accepted 15 March 2004

Abstract

The organic–inorganic hybrid nanoparticles entrapping oligodeoxynucleotide (ODN) or siRNA were prepared through the self-associating phenomenon of the block copolymer, poly(ethylene glycol)-*block*-poly(aspartic acid) (PEG-PAA), with calcium phosphate. The nanoparticles have diameters in the range of several hundreds of nanometers depending on the PEG-PAA concentration and revealed excellent colloidal stability due to the steric repulsion effect of the PEG layer surrounding the calcium phosphate core. The loading capacities of ODN and siRNA were fairly high, reaching almost 100% under optimal conditions. The flowcytometric analysis and confocal microscopy observation indicated that the hybrid nanoparticles loaded with ODN were taken up by the cells through the endocytosis mechanism. Furthermore, the calcium phosphate core dissociates in the intracellular environment with appreciably lowered calcium ion concentration compared to the exterior, allowing the release of the incorporated ODN and siRNA in a controlled manner. Eventually, effective intracellular delivery and nuclear localization of these nucleic acid-based drugs were evidenced through the observation of laser confocal microscopy using FITC-labeled ODN. This smart ion-sensitive characteristic of hybrid nanoparticles was further demonstrated by the appreciable silencing of reporter gene expression by siRNA incorporated in the nanoparticles.

Keywords: Polymeric micelle; Block copolymer; Gene silencing; Calcium phosphate; siRNA

1. Introduction

The therapeutic performance of nucleic acid based drugs significantly depends on the capability of carrier systems because of their fragility, impermeability to the cellular membrane and undesirable biodistribution [1–9]. Carrier systems should protect these nucleic acid based drugs in the harsh environment of the extracellular fluids, while inside the cells they should release incorporated drugs at a reasonable rate to maintain intracellular concentration sufficient to form a complex with the target molecules such as mRNA. Sensitivity to the intracellular envi-

* Corresponding author. Biomaterials Center, National Institute for Materials Science, 1-1 Namiki, Tsukuba, Ibaraki 305-0044, Japan.
E-mail address: kataoka@bmw.t.u-tokyo.ac.jp (K. Kataoka).

0168-3659/$ - see front matter © 2004 Elsevier B.V. All rights reserved.
doi:10.1016/j.jconrel.2004.03.031

ronment of the carrier is a key concept to fulfill this critical requirement, such that the carrier undergoes structural change in response to the drastic gap in the concentrations of the chemicals and ions between both sides of the plasma membrane [10–13]. It is important to note the 10^4 times reduction of the free calcium ion concentration as well as the 40–70 times increase in the phosphate ion concentration in the intracellular compartment compared to the extracellular milieu, leading us to design an ion-sensitive nanoparticulate delivery system with the core of calcium phosphate (CaP). Polymeric micelles were chosen as a base material because this system has already shown long-circulating properties and has been successfully utilized for systemic administration of small molecular drugs including anticancer drugs [14–18]. The characteristic size in the range of several tens to hundreds of nanometers and the surrounding hydrophilic polymer layers endow them with the ability to avoid undesirable foreign-body recognition in biological entities and to achieve effective extravasation from the blood stream to tumorous and inflammetry tissues through the enhanced permeation and retention (EPR) effect, resulting in the high drug accumulation to the target site. On the other hand, inner cores play a pivotal role in the stability of the micelles as well as the accommodation of the cargo molecules. Thus, engineering the core properties would lead to the development of functional micelles with environment-sensitivity, retaining the benefit of the biocompatible shell layer [19].

Here, the micellization behavior of block copolymers was utilized to prepare organic–inorganic hybrid nanoparticles with a core-shell structure: core composed of nanocrystals of CaP surrounded by a hydrophilic tethered layer of poly(ethylene glycol) (PEG). As reported in the previous communication, the mixing of calcium and phosphate solutions in the presence of oligodeoxynucleotides (ODN) and poly(ethylene glycol)-*block*-poly(aspartic acid) (PEG-PAA) led to the spontaneous formation of ODN-incorporated hybrid nanoparticles with narrow distribution in the range of tens to several hundreds of nanometers [20]. On the other hand, in the absence of PEG-PAA, ODN/CaP complexes form precipitates within tens of seconds after the mixing of the solutions. The underlying concept is to prevent crystal growth through the absorption of the PAA segment of PEG-PAA on the crystal surface. It should be noted that CaP, especially hydroxyapatite, is one of the most widely used biomaterials in medical application, due to its excellent biocompatibility and similarity to biological inorganic materials such as bone and teeth. A wide variety of molecules including proteins, nucleic acid and low-molecular-weight drugs have a substantial binding ability to CaP, making it feasible as a controlled release matrix [21,22]. Nevertheless, nanoparticulate formulation of calcium phosphate was difficult to achieve because, after the initial mixing of calcium and phosphate solutions, the growth of the CaP crystal is uncontrollably rapid to induce large precipitates. The use of a PEG-polycarboxylate block copolymer, such as PEG-PAA, overcomes this issue of crystal over-growth, allowing us to obtain a smart nanocarrier with intracellular ion sensitivity. The objective of this study is to characterize the CaP/PEG-PAA hybrid nanoparticles incorporating oligonucleotides or siRNA, particularly focusing on their cellular uptake and the calcium and phosphate ion-sensitive release of the entrapped molecules.

2. Materials and methods

2.1. Materials

Poly(ethylene glycol)-block-poly(aspartic acid) was synthesized as previously described with slight modification [23]. Briefly, the *N*-carboxy anhydride of β-benzyl L-aspartate (BLA-NCA) was synthesized by the Fuchs-Farthing method. The polymerization of BLA-NCA was initiated from the terminal amino group of α-methoxy-ω-aminoPEG (Mw 12,000) (Nippon Oil and Fat) in CH_2Cl_2. The degree of the polymerization was determined to be 24 by ^{1}H-NMR measurements. Alkaline deprotection of the side groups was performed in 0.1 N sodium hydroxide solution. Under this deprotection condition, the PAA segment of PEG-PAA is isomerized and racemized, resulting in the formation of poly(α,β-DL-aspartic acid). Phosphodiester ODN for GL3 luciferase (5′-ATGCCCATACTGTTGAG-3′ [24]) was purchased from Sigma Genosys Japan K.K. The annealed siRNA targeting GL3 luciferase (sense: 5′-CUUACGCUGAGUACUUCGATT-3′, an-

tisense: 3′-TTGAAUGCGACUCAUGAAGCU-5̄′ [25]) and control (non-silencing) siRNA (sense: 5′-UUCUCCGAACGUGUCACGUTT-3′, antisense: 3′-TTAAGAGGCUUGCACAGUGCA-5′) were obtained from Qiagen. Sodium azide and 2-deoxy-glucose were purchased from Wako. Reporter vectors, pGL3-control and pRL-TK, from Promega were amplified by *Escherichia coli* strain and purified by the Hispeed Plasmid Maxi Kit (Qiagen). Dual-Glo Luciferase Assay System was purchased from Promega. Salmon sperm DNA was solubilized by sonication using the Tomy Ultrasonic Disruptor (UD-2000). Poly(α,β-DL-aspartic acid) was purchased from Sigma. All other reagents were used without further purification.

2.2. Sample preparation

A solution of 2.5 M $CaCl_2$ was added to a solution of ODN or siRNA in a buffer (1 mM Tris–HCl, 0.1 mM EDTA, pH 7.6) to a final volume (Ca^{2+} 250 mM, ODN 70 μg/ml (siRNA 74 μg/ml)). One volume of this 2 × Ca/ODN solution was quickly added to an equal volume of 2 × Hepes/phosphate/PEG-PAA solution (140 mM NaCl, 50 mM HEPES, 3.0 or 6.0 mM Na_2HPO_4, PEG-PAA, pH 7.1). The mixed solutions were vigorously stirred by a vortex mixer for a few seconds and incubated at 37 °C for 24 h.

2.3. Particle size determination

Dynamic light scattering measurements were carried out for the particle solutions using a Photal dynamic laser scattering DLS-7000DL spectrometer (Otsuka Electronics) equipped with an argon laser (488 nm). The scattering data was analyzed by the cumulant method [26] to obtain hydrodynamic diameter and polydispersity index, which is defined by the normalized *z*-average variance of the distribution of the diffusion coefficient. *z*-Averaged size distributions of the particles were determined by the histogram methods [27].

2.4. Determination of ODN/siRNA content

The sample solutions (200 μl) were centrifuged at 15,000 × *g* for 30 min to precipitate the nanoparticles. Supernatants (100 μl) were carefully removed to determine the ODN/siRNA concentration by absorbance at 260 nm. The percentage of the loaded ODN/siRNA was calculated by subtracting the ODN/siRNA concentration in the supernatant from the total concentration.

2.5. X-ray diffraction (XRD) and Fourier transform infrared (FTIR) measurements

The crystalline phase of the precipitate formed in the absence of PEG-PAA and ODN was determined by an X-ray diffractometer (PW-1700, Philips) with CuK_α radiation. The scanning range of the samples was from 4° to 70°. The accelerating voltage and current were 40 kV and 40 mA, respectively.

The precipitate formed in the absence of PEG-PAA and ODN and the hybrid nanoparticle samples obtained after centrifugation were dried in vacuo overnight. The infrared spectra of those specimens and PEG-PAA were recorded using KBr pellets on a Spectrum2000 FTIR spectrophotometer (Perkin Elmer) over the 4000–400 cm^{-1} region with a 1-cm^{-1} resolution. Each spectrum was scanned over 64 times to increase the signal-to-noise ratio.

2.6. Kinetics of dissolution of the hybrid nanoparticles

The nanoparticle solutions prepared under the polymer concentration of 420, 560 and 700 μg/ml were centrifuged at 15,000 × *g* for 30 min. The supernatants were carefully removed, and the precipitates were resuspended in the aqueous buffer solutions containing calcium and phosphate ions with concentrations similar to intracellular fluids ($CaCl_2$ 100 nM, Na_2HPO_4 40 mM, pH 7.4, NaCl 140 mM) or extracellular fluids ($CaCl_2$ 2 mM, Na_2HPO_4 1 mM, Tris 25 mM, pH 7.4, NaCl 140 mM). Each solution (100 μl) was dialyzed against 1 l of the respective solutions at 37 °C using MicroDispoDialyzers (MwCO: 15,000, Spectrum). At the desired time, the absorbance of the nanoparticle solutions at 260 nm was measured using a microplate reader (GENios, TECAN).

2.7. Flowcytometric analysis of cellular uptake of the hybrid nanoparticles

HeLa cells were plated at a density of ~ 2×10^4 cells/well in 24-well plates 24 h before the start of

the experiment. Fifty microliters of the sample solutions of FITC labeled-ODN with the scrambled sequence (35 μg/ml) or hybrid nanoparticles containing FITC-ODN (ODN 35 μg/ml, Ca 125 mM, phosphate 3.0 mM, polymer 560 μg/ml) were added to the medium containing 10% serum (450 μl). At the desired incubation time, the cells were washed with PBS, trypsinized and suspended in 1–2 ml of PBS. Approximately $5-10\times10^3$ cells from each sample were subjected to flowcytometric analysis. The total mean fluorescence of the untreated controls was set to 0.48, and the gate used for the analysis of the treated cells was set to include 1% of the most brightly fluorescent control cells as background.

For inhibition studies, HeLa cells were pretreated at 4 °C or in the medium containing 10 mM of sodium azide and 25 mM of 2-deoxyglucose at 37 °C for 0.5 h. The sample solutions of nanoparticles formed at 560 μg/ml of PEG-PAA were then added to the medium and incubated at 4 °C or in the presence of 10 mM azide and 25 mM 2-deoxyglucose for 4 h. The flowcytometric analysis was performed as previously described.

2.8. Confocal microscopy

HeLa cells were cultured on 35-mm glass-base dishes at $\sim 2\times10^4$ cells/dish. To the 900 μl of the medium was added 100 μl of sample solution of FITC-labeled free ODN or nanoparticle solution containing FITC-ODN prepared under the same conditions as for the flowcytometric analysis. For the investigation of the intracellular behavior, a glycerol shock was applied to cells after the contact with the nanoparticle solution. The glycerol shock was applied by the following procedure: the medium was aspirated and the cells were rinsed once with 2 ml serum-free culture medium. The addition of 1.5 ml of 15 % (w/v) glycerol/PBS was followed by incubation for 30 s at room temperature. The medium was aspirated and the cells were rinsed with a serum-free medium. After the incubation for 30 min, 50 μl of Hoechst 33258 solution (1 mg/ml) was added to the medium and further incubated for 15 min, and then the cells were rinsed twice with PBS, followed by the confocal microscopy observation.

2.9. Biological activity of incorporated siRNA

At the density of 8×10^4 cells/well in a 96-well plate, 293 cells were plated and grown overnight. Using lipofectAMINE™ reagent according to the manufacturer's protocol, pGL3-control (25 ng/well) and pRL-TK vectors (75 ng/well) were transfected to the cells. After 4 h of transfection, the medium was removed, and the cells were washed with DMEM two times and incubated in a serum-containing medium for 2 h. Forty microliters of siRNA samples were diluted with 360 μl of the medium. After replacement with a fresh medium (50 μl), a siRNA sample (50 μl) was added to each well and incubated for 24 h in DMEM containing 10% FCS and 100 μM of chloroquine (100 μl). Naked siRNA, nanoparticles without siRNA and nanoparticles entrapping non-silencing siRNA were used as control. The final concentration of the siRNA was 125 nM. Luciferase activities were determined using the Dual Glo Luciferase Assay System from Promega.

3. Results and discussion

3.1. Formation of calcium phosphate/PEG-PAA hybrid nanoparticles

The organic–inorganic hybrid nanoparticles of calcium phosphate (CaP) were prepared in the presence of the block copolymer, PEG-PAA, which has the poly(aspartic acid) (PAA) segment with the high binding affinity to CaP and the nonionic and hydrophilic segment of PEG with the steric stabilization function. The resulting nanoparticles should have the core-shell structure with the core of CaP/PAA and the shell of PEG. PEG-PAA with the PEG segment having a molecular weight (Mw) of 12,000 was used in the present study, because polymeric micelles with PEG Mw = 12,000 generally show improved pharmacokinetics after intravenous injection as compared to those with PEG Mw = 5000 [28]. Loading of the ODN or siRNA molecules into the nanoparticles was achieved by the addition of these molecules into the calcium solution before mixing with the phosphate/PEG-PAA solution [20].

The sizes of the ODN-incorporated nanoparticles formed at 1.5 and 3.0 mM phosphate with varying

concentrations of PEG-PAA were determined by the dynamic light-scattering measurements and are shown in Fig. 1a. Here, the nanoscaled hybrid particles with high colloidal stability were easily obtained. The diameters of the particles ranged from 100 to 300 nm depending on the PEG-PAA and phosphate concentrations. At 1.5 mM phosphate, the diameters revealed the minimum value at 170 μg/ml of PEG-PAA, and the decrease in the PEG-PAA concentration from this point caused a rapid increase in the diameters, resulting in the formation of precipitates. This probably occurs because the amount of PEG-PAA is not sufficient to entirely cover the surface of CaP in the concentration range below the critical concentration of PEG-PAA. Similarly, the minimum diameter was observed at 350 μg/ml of PEG-PAA at 3.0 mM phosphate. Notably, the polydispersity indices were below 0.1 for all of the nanoparticles formed above these critical concentrations, indicating that the particles have very narrow size distribution as typically seen in Fig. 1b,c. When doubling the phosphate concentration from 1.5 to 3.0 mM, twice the amount of PEG-PAA was required to obtain similar sizes of the nanoparticles. Considering that most of the phosphate ions should participate in the formation of the CaP crystal in the presence of excess calcium ion, this result indicates that the similar structure of the nanoparticles is formed despite the difference in the initial

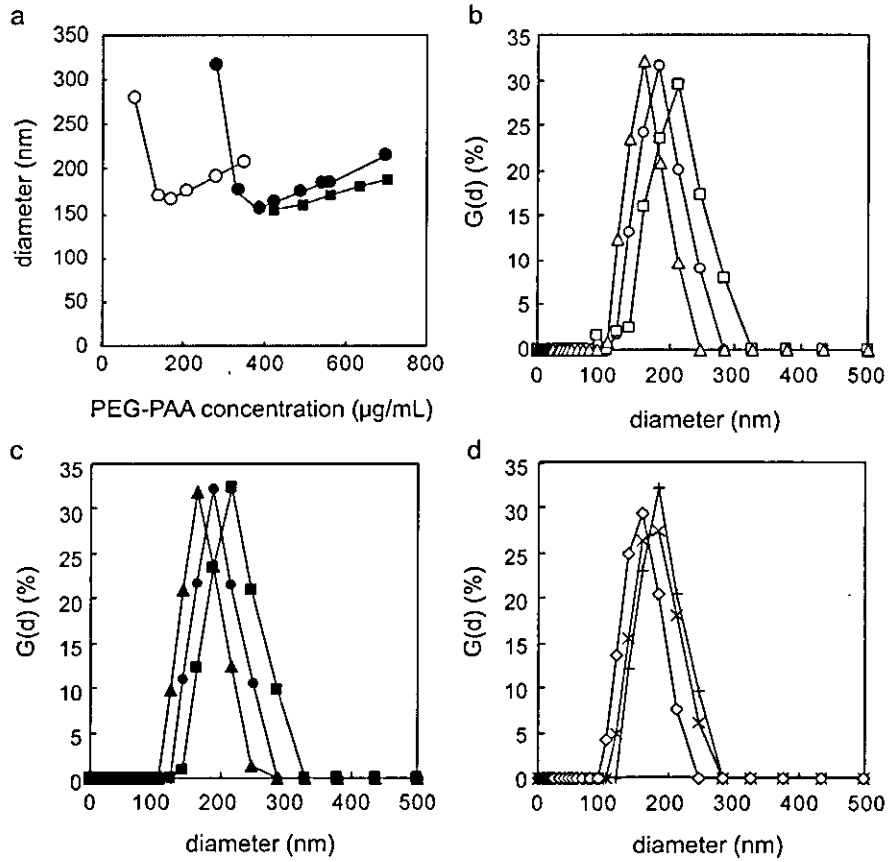

Fig. 1. Size and size distribution of the hybrid nanoparticles entrapping ODN and siRNA determined by DLS measurements. (a) Effect of PEG-PAA and phosphate concentrations on the size of the hybrid nanoparticles. (○) ODN at 1.5 mM phosphate, (●) ODN at 3.0 mM phosphate, (■) siRNA at 3.0 mM phosphate. (b–d) z-Averaged size distribution for the hybrid nanoparticles entrapping ODN at 1.5 mM phosphate (b), ODN at 3.0 mM phosphate (c) and siRNA at 3.0 mM phosphate (d). PEG-PAA concentrations (μg/ml): (△) 170, (○) 280, (□) 350, (▲) 420, (●) 560, (■) 700, (◇) 420, (×), 560, (+) 700.

concentrations of the components. Moreover, the diameters of the hybrid nanoparticles entrapping siRNA formed at 3.0 mM phosphate were similar to those entrapping ODN (Fig. 1a and d), suggesting similar structures of the nanoparticles for both nucleic acid drugs.

The amount of ODN or siRNA associated with the nanoparticles was determined by the centrifugation assay, in which the absorbance of the supernatant at 260 nm was measured after centrifugation at 15,000 × g for 30 min. Fig. 2 illustrates that ODN can be effectively entrapped in the nanoparticles, and more than 97% of ODN loading was achieved at 3.0 mM phosphate. The amounts of loaded ODN were higher for nanoparticles formed at 3.0 mM phosphate than those at 1.5 mM. The increased amount of phosphate ion, and hence CaP, is likely to raise the total capacity of ODN loading whose concentration is constant in these experiments. As the PEG-PAA concentration increased at 1.5 mM phosphate, the amount of incorporated ODN substantially decreased, suggesting that exclusion of ODN occurs due to the competitive binding to CaP between PEG-PAA and ODN. siRNA was incorporated to a lesser extent than ODN, but still more than 78% under the experimental conditions. The nucleoside unit concentrations of ODN and siRNA under these experimental conditions were almost identical: 105 and 106 μM for ODN and siRNA, respectively. This result indicates that the structural difference between single-stranded ODN and double-stranded siRNA may define their incorporating efficacy into the nanoparticles.

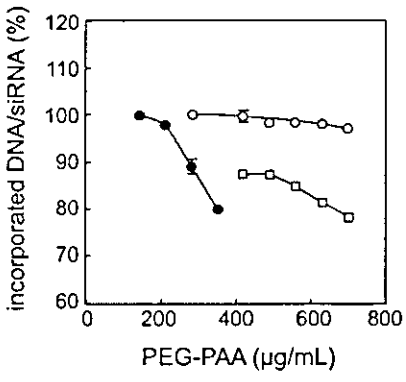

Fig. 2. Percentage of ODN and siRNA loaded in the nanoparticles formed at the varying PEG-PAA and phosphate concentrations. (●) ODN at 1.5 mM, (○) ODN at 3.0 mM, (□) siRNA at 3.0 mM.

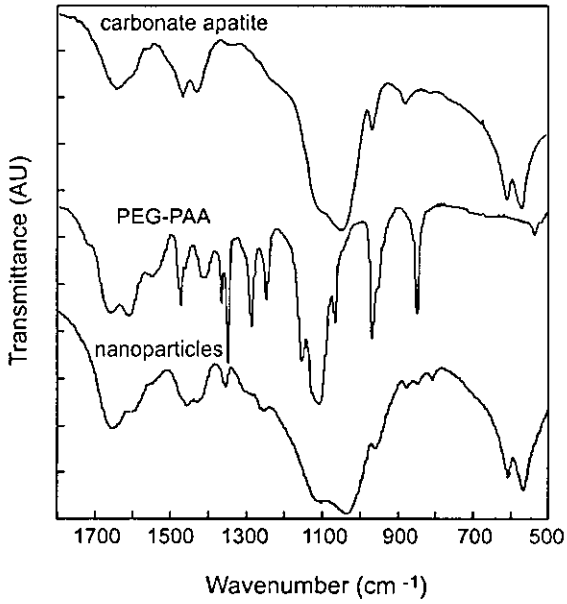

Fig. 3. FTIR spectra of carbonate apatite, PEG-PAA and hybrid nanoparticles formed at 560 μg/ml of PEG-PAA.

3.2. Characterization of the hybrid nanoparticles

To characterize the structure of the CaP core of the nanoparticles, XRD and FTIR measurements were carried out. First, the phase of CaP was elucidated for the model samples prepared in the presence and absence of poly(α,β-aspartic acid) (homopolymer) and salmon sperm DNA. XRD patterns of these samples gave the peak with broad band width, indicating the formation of hydroxyapatite with low crystallinity (data not shown). This XRD result on CaP/PAA/DNA samples suggests that a similar structure would form in the core of the hybrid nanoparticles of CaP/PEG-PAA/ODN or siRNA. This is supported by the FTIR spectra of the hybrid nanoparticles prepared in the presence of 560 μg/ml of PEG-PAA and 35 μg/ml of ODN (Fig. 3), revealing typical carbonate-containing apatitic features (PO_4^{3-} bands at 1000–1100 and 550–650 cm^{-1}; CO_3^{2-} bands at 875 and 1400–1500 cm^{-1}). The increase in the absorption bands at 1630–1700 cm^{-1} for the hybrid nanoparticles can be attributed to the C=C and

C=N stretching bands of ODN bases [29] and the amide I band of the PAA segment of PEG-PAA. Similar results were obtained for the nanoparticles formed at 420 and 700 μg/ml of PEG-PAA. Furthermore, the pH was maintained at 7.4 during the nanoparticle synthesis so as to be in a favorable condition for hydroxyapatite formation [30]. Consequently, all of these results reasonably support that the core phase of the hybrid nanoparticles is likely to be the carbonate apatite with low crystallinity.

Once inside the cells, the hybrid nanoparticles have to release the loaded oligonucleotides (ODN or siRNA) to the intracellular environment to exert their biological effect. As for the triggering stimulus to release the oligonucleotides, the difference between the intra- and extracellular concentrations of calcium and phosphate ions was focused, because these concentrations mainly influence the dissolution behavior of the CaP crystals. The extracellular concentration of free calcium ion is approximately 2 mM, while that in the intracellular fluid abruptly decreased to that on the order of 100 nM [31]. On the other hand, the concentration increases from 1 to 40–70 mM for the phosphate ion through an environment change from the extracellular to intracellular compartment [32]. These 20,000-fold lower calcium and 40–70-fold higher phosphate ion concentrations in the intracellular compartment compared to the extracellular fluid are likely to lead to the selective dissolution of the CaP nanoparticles inside the cells. To assess this feasible dissolution, the dialysis assay was initially performed to determine whether the nanoparticles can be dissolved under the conditions mimicking the intracellular environment.

The nanoparticle solutions were dialyzed against dialysates with calcium and phosphate ion concentrations adjusted to intra- or extracellular values. An excess volume of dialysate was used to avoid the concentration change accompanied by the dissolution of the nanoparticles. Fig. 4 shows the time course of change in the absorbance at 260 nm for ODN-incorporated nanoparticles formed at 420, 560 and 700 μg/ml of PEG-PAA. Obviously, the absorbance decreased with incubation time under the conditions containing 100 nM of calcium and 40 mM of phosphate (intracellular condition) mainly due to the decreased Rayleigh scattering through particle dissolution. The final absorbance lower than 1.0 after 24 h of incubation shows that the ODN release into the dialysate accompanied by particle dissolution also contributes to the decrease in total absorbance at 260 nm, because the absorbance of ODN in the initial solution was set at 1.0. On the other hand, the absorbance of the solutions was almost unchanged for the sample prepared at 560 and 700 μg/ml of PEG-PAA when they were dialyzed against a dialysate containing 2 mM calcium and 1 mM phosphate (extracellular condition), indicating the high colloidal stability of the nanoparticles under this condition. The continuous increase in the absorbance for the sample prepared at 420 μg/ml of PEG-PAA might be due to the slow secondary agglomerization of the nanoparticles, because of the insufficient

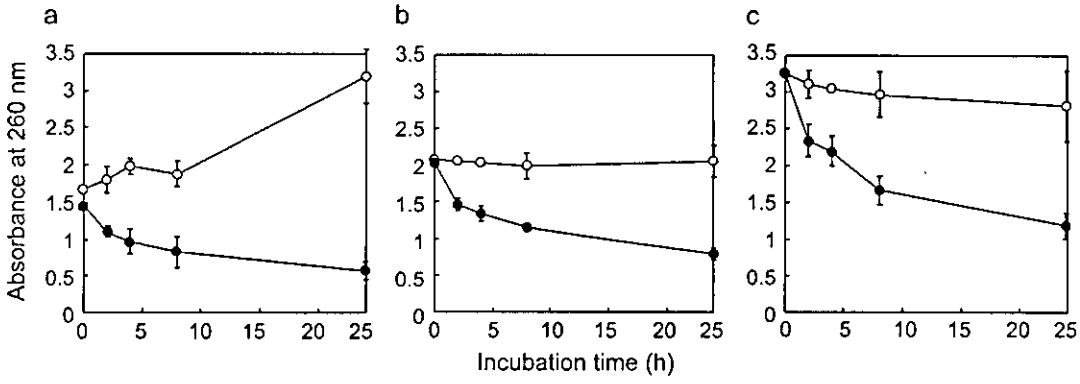

Fig. 4. Dissociation kinetics of the hybrid nanoparticles under the conditions mimicking the intracellular (●) and extracellular (○) compartments. PEG-PAA concentrations; (a) 420 μg/ml, (b) 560 μg/ml, (c) 700 μg/ml. The mean ± S.D. of three experiments is presented.

colloidal stability resulting from the low density of the steric stabilizing layer of PEG. Eventually, these results of model dialysis experiments strongly suggest that hybrid nanoparticles with appropriate composition are indeed likely to selectively dissociate in the intracellular environment.

3.3. Study on the cellular uptake

The flowcytometric analysis was performed to evaluate the time course of the cellular uptake of 5′-FITC-labeled ODN (FITC-ODN) entrapped in the nanoparticles. The cytofluorogram gave a single peak, which gradually shifted toward the higher fluorescent region with incubation time. This result suggests the uniform cellular uptake process of ODN-incorporated hybrid nanoparticles. The mean cellular fluorescence as well as the percentage of FITC-positive cells is shown in Fig. 5a as a function of time. No remarkable increase in fluorescence was observed for the cells treated with free FITC-ODN. In marked contrast, fast and effective ODN uptake by HeLa cells was achieved using the nanoparticles as carrier systems, and almost all cells internalized ODN after 4 h of incubation. These results clearly demonstrate that inclusion into the nanoparticles is necessary for the efficient uptake of ODN molecules into HeLa cells under these experimental conditions.

Fig. 5b,c shows the percentage and fluorescence intensity of the FITC-positive cells after 4 h of incubation under different conditions. The fluorescence intensities are shown as a relative value to that of cells treated at 37 °C with nanoparticles formed at 560 μg/ml. The nanoparticles formed at 420 and 560 μg/ml of PEG-PAA had similar effect on the uptake of ODN, while the amount of internalized ODN was lower for the nanoparticles formed at 700 μg/ml. This might be ascribed to the combining effect of the larger diameter and the possible higher density of the PEG segment on the surface of the nanoparticles at 700 μg/ml (Fig. 5b). To clarify the role of the energy-dependent process in the ODN uptake, the cells were incubated at 4 °C or treated with a mixture of metabolic inhibitors, azide and 2-deoxyglucose (DG) [33] (Fig. 5c). Low-temperature incubation at 4 °C significantly reduced the percentage of cells in the gate region as well as the relative fluorescence intensity, compared to the normal conditions at 37 °C. Treatment with the

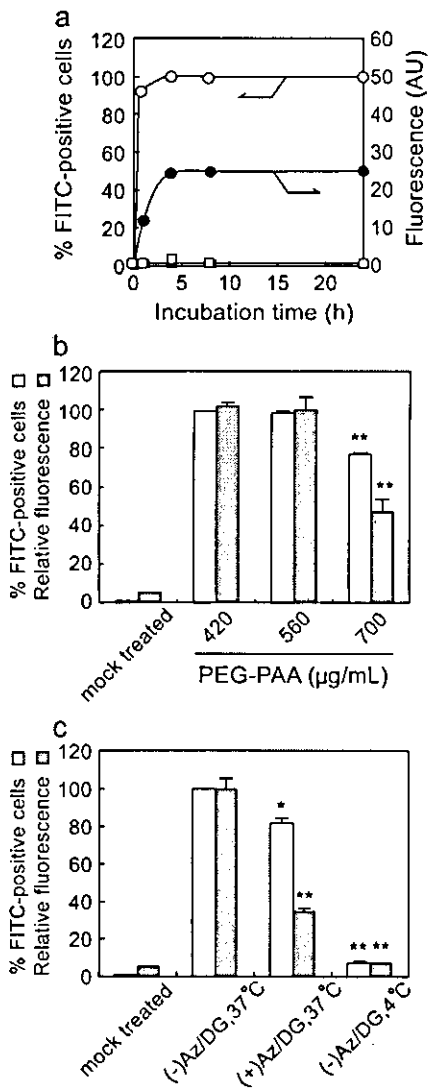

Fig. 5. (a) Cellular uptake of free and nanoparticle-loaded ODN by HeLa cells at 37 °C. (□, ■) free ODN and (○, ●) ODN loaded in the nanoparticles formed at 560 μg/ml of PEG-PAA. Percentage of the cells in the gate region (closed symbols) and mean fluorescence intensity (open symbols) were determined as a function of time. (b) Effect of PEG-PAA concentration on the uptake of nanoparticle-loaded ODN. Fluorescence intensity was expressed as a relative value to that of the cells incubated with nanoparticles formed at 560 μg/ml. $^{*}p<0.05$ and $^{**}p<0.01$ versus cells treated with the hybrid nanoparticles formed at 560 μg/ml of PEG-PAA. (c) Effect of inhibitors and temperature on the uptake of nanoparticle-loaded ODN. The hybrid nanoparticles were formed at 560 μg/ml of PEG-PAA. Az/DG; azide and 2-deoxyglucose. $^{*}p<0.01$ and $^{**}p<0.001$ versus cells incubated at 37 °C without the inhibitors. The mean ± S.E.M. of three experiments is presented.

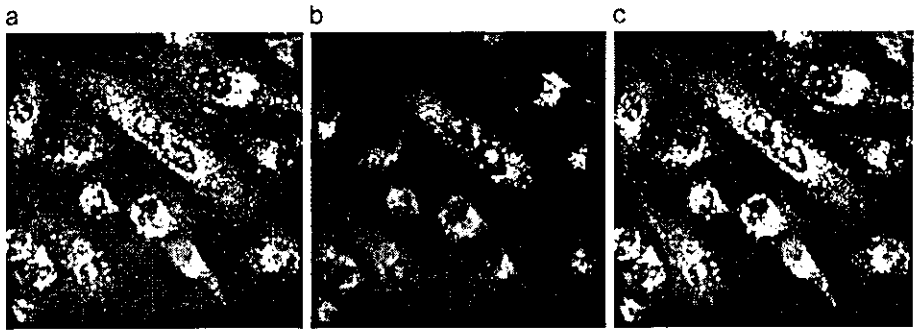

Fig. 6. Intracellular distribution of FITC-labeled ODN incorporated in the hybrid nanoparticles. HeLa cells were incubated with the hybrid nanoparticles formed at 560 μg/ml of PEG-PAA. Endosome/lysosomes were stained with TexRed dextran. (a) FITC-labeled ODN, (b) TexRed dextran, (c) an overlay of (a) to (b).

mixture of azide and DG also reduced the percentage of FITC-positive cells and the relative fluorescence intensity to 81% and 34%, respectively, as compared to those in the absence of these reagents. These results suggest that the nanoparticles are likely to be taken up by the cells through an energy-dependent endocytotic pathway.

The intracellular distribution of the FITC-ODN was then investigated by laser confocal microscopy. In accordance with the results of the flowcytometric analysis, free FITC-ODN added to the culture media was poorly internalized, and the confocal images showed very limited localization into punctate cytoplasmic regions probably corresponding to an endocytic compartment (data not shown). On the other hand, the bright, punctate fluorescence of FITC was mainly observed for the cells treated with the nanoparticles carrying FITC-ODN prepared at 560 μg/ml of PEG-PAA and 3.0 mM phosphate (Fig. 6a). Yellow color in the merged picture (Fig. 6c) suggests the co-localization of the FITC-ODN and TexRed-dextran (Fig. 6b), an endosome marker, supporting the endocytotic pathway for the nanoparticle uptake. Similar results were obtained for the nanoparticles prepared at 420 and 700 μg/ml of PEG-PAA.

The glycerol shock was then applied to enhance the transport of the endosomal trapped nanoparticles into the cytoplasm through the destabilization of the endosomal membrane [34]. As shown in the microscope image (Fig. 7a), the fluorescence of FITC-ODN was distributed in the cytoplasm and even in the nucleus region, which is indicated from the merged picture (Fig. 7c) of the FITC image (Fig. 7a) and Hoechst 33258 image (Fig. 7b) known to selectively stain the nucleus region. Considering the fact that the nanoparticle (~ 170 nm) has a substantially larger

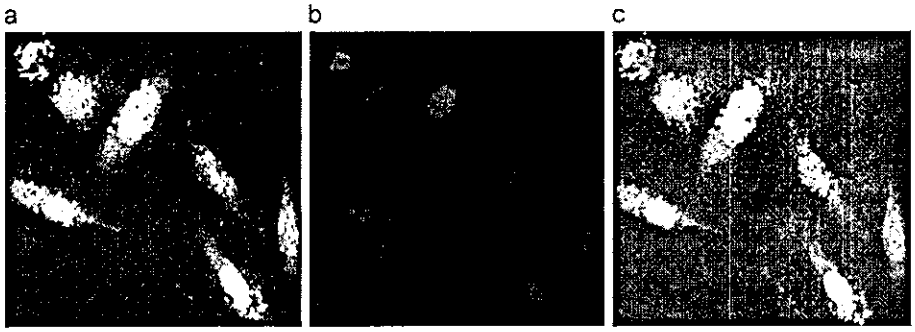

Fig. 7. Intracellular distribution of FITC-labeled ODN incorporated in the hybrid nanoparticles after glycerol shock. HeLa cells were incubated with the hybrid nanoparticles formed at 560 μg/ml of PEG-PAA, followed by glycerol addition at 0.5 h before observation. Nuclei were stained with Hoechst33258 dye. (a) FITC-labeled ODN, (b) Hoechst33258 (nucleus), (c) an overlay of (a) to (b).